Geochronology, geochemistry and tectonic implications of early Carboniferous plutons in the southwestern Alxa Block

Zeng-Zhen Wang[1,2], Xuan-Hua Chen[1,2], Zhao-Gang Shao[1,2] (ORCID), Bing Li[1,2], Hong-Xu Chen[1,2], Wei-Cui Ding[1,2], Yao-Yao Zhang[1,2] and Yong-Chao Wang[1,2]

[1]Chinese Academy of Geological Sciences, Beijing 100037, China and [2]SinoProbe Center, Chinese Academy of Geological Sciences and China Geological Survey, Beijing 100037, China

Abstract

The southeastern Central Asian Orogenic Belt (CAOB) records the assembly process between several micro-continental blocks and the North China Craton (NCC), with the consumption of the Paleo-Asian Ocean (PAO), but whether the S-wards subduction of the PAO beneath the northern NCC was ongoing during Carboniferous–Permian time is still being debated. A key issue to resolve this controversy is whether the Carboniferous magmatism in the northern NCC was continental arc magmatism. The Alxa Block is the western segment of the northern NCC and contiguous to the southeastern CAOB, and their Carboniferous–Permian magmatism could have occurred in similar tectonic settings. In this contribution, new zircon U–Pb ages, elemental geochemistry and Sr–Nd isotopic analyses are presented for three early Carboniferous granitic plutons in the southwestern Alxa Block. Two newly identified aluminous A-type granites, an alkali-feldspar granite (331.6 ± 1.6 Ma) and a monzogranite (331.8 ± 1.7 Ma), exhibit juvenile and radiogenic Sr–Nd isotopic features, respectively. Although a granodiorite (326.2 ± 6.6 Ma) is characterized by high Sr/Y ratios (97.4–139.9), which is generally treated as an adikitic feature, this sample has highly radiogenic Sr–Nd isotopes and displays significantly higher K_2O/Na_2O ratios than typical adakites. These three granites were probably derived from the partial melting of Precambrian continental crustal sources heated by upwelling asthenosphere in lithospheric extensional setting. Regionally, both the Alxa Block and the southeastern CAOB are characterized by the formation of early Carboniferous extension-related magmatic rocks but lack coeval sedimentary deposits, suggesting a uniform lithospheric extensional setting rather than a simple continental arc.

CAMBRIDGE
UNIVERSITY PRESS

1. Introduction

The Phanerozoic Central Asian Orogenic Belt (CAOB), one of the largest long-lived accretionary orogens worldwide, is situated to the north of the Tarim–North China cratons (Fig. 1a) and formed by complex subduction, accretion and collision processes related to the consumption of the Paleo-Asian Ocean (PAO), with significant crustal growth (Han *et al.* 1997, 2011; Jahn *et al.* 2000; Wu *et al.* 2003; Windley *et al.* 2007; Xiao *et al.* 2018). The southeastern CAOB records the Palaeozoic amalgamation between the North China Craton (NCC) in the south and Mongolia, Hunshandake and Songliao blocks within the CAOB in the north (Xu *et al.* 2013; Zhao *et al.* 2018; Zhou *et al.* 2018). The Permian–Early Triassic Solonker suture (Solonker–Xar Moron–Changchun suture) contains the youngest ophiolites within the southeastern CAOB and is usually regarded as the terminal closure site of the PAO (Eizenhöfer & Zhao, 2018; Wilde & Zhou, 2015; Xiao *et al.* 2003). However, when and how the PAO finally closed in the southeastern CAOB is still controversial, and different opinions can be grouped into three models.

In the first set of models, the subduction of the PAO was continuous from the early Palaeozoic Era to Late Permian–Early Triassic time and led to the successive accretion of micro-continental blocks and magmatic arcs to the northern NCC, with the northern margin of the NCC as a continental arc during Carboniferous–Permian time and the Solonker suture as the final closure site of the PAO (e.g. Xiao *et al.* 2003, 2009*b*, 2018; Zhang *et al.* 2014, 2016*d*). The second set of models propose the Late Devonian–early Carboniferous closure of the PAO, with the southeastern CAOB in a post-collisional setting since then (e.g. Xu *et al.* 2013; Tong *et al.* 2015; Zhang *et al.* 2015*b*). The third set of models infer that the large-scale PAO closed before the Late Devonian Epoch, but a new orogenic cycle began with intra-continental rifting within the southeastern CAOB during early Carboniferous time and resulted in the formation of a Red-Sea-like limited ocean basin, with the Solonker suture marking its closure during the Early Triassic Epoch (e.g. Zhang *et al.* 2015*a*; Luo *et al.* 2016; Pang *et al.* 2016; Zhao *et al.* 2017; Xu *et al.* 2018). In the third model, the lithospheric extension may be triggered by slab
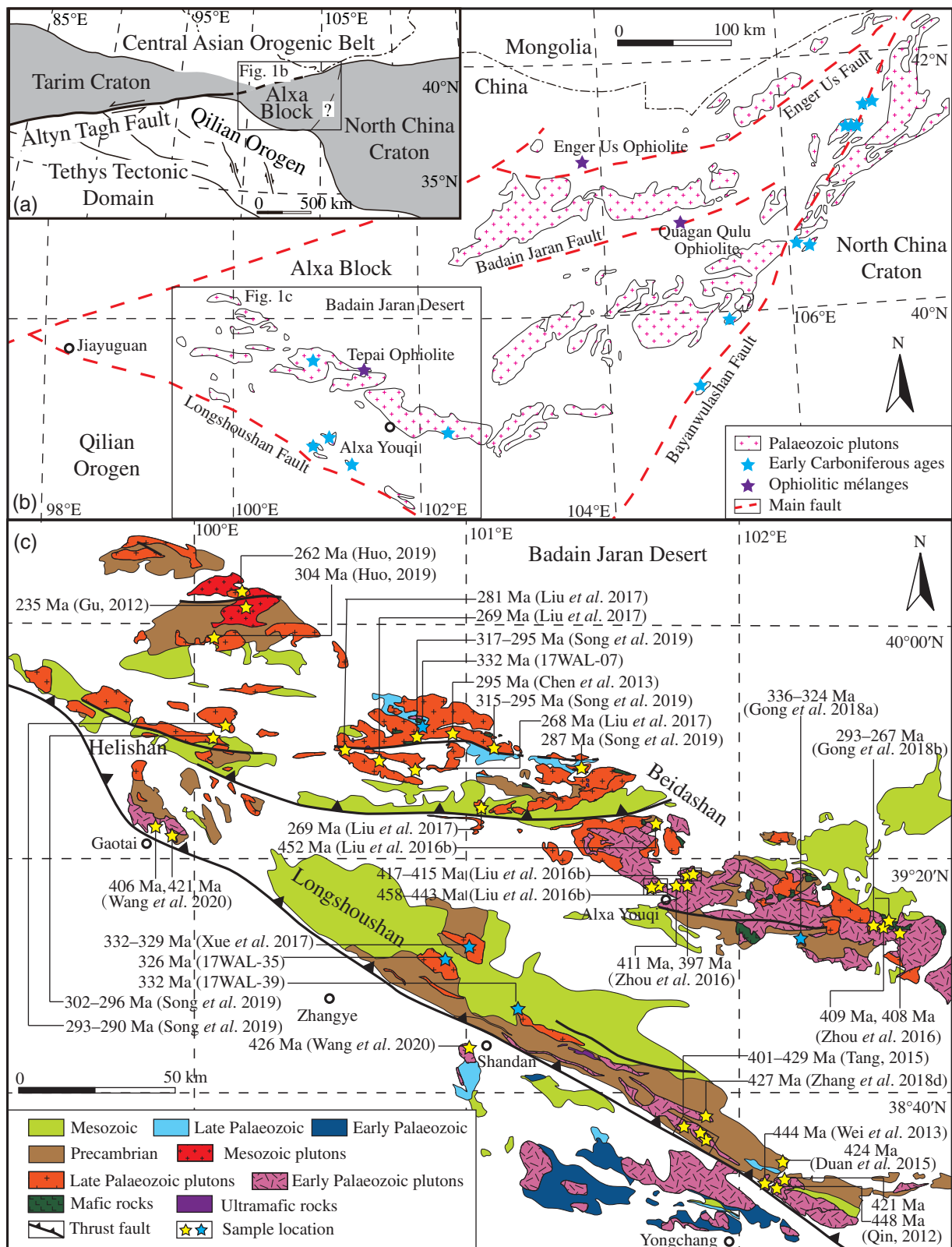
Fig. 1. (Colour online) (a) Tectonic location of the Alxa Block. (b) Schematic geological map showing the distribution of Palaeozoic intrusions and ophiolitic mélanges in the Alxa Block (modified after Dan *et al.* 2014). (c) Simplified geological map of the southwestern Alxa Block (modified after Wang *et al.* 2020).

break-off (Kozlovsky *et al.* 2015; Zhang *et al.* 2012*a*) and enhanced by slab avalanche-driven wet mantle upwelling rising from the hydrous mantle transition zone (Wang *et al.* 2015*a*, 2016*a*).

To test the likelihood of one of these geodynamic models, a key question is whether the Carboniferous–Permian tectono-magmatic activity of the southeastern CAOB was dominated by
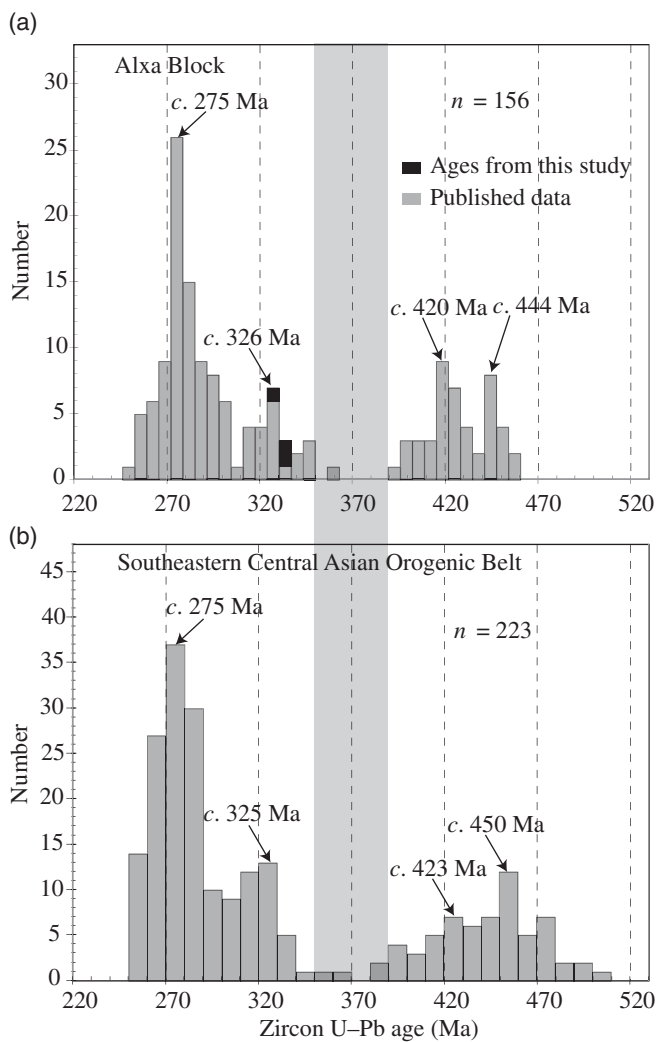
(a)

(b)

Fig. 2. Statistical histograms of zircon U–Pb ages of Palaeozoic magmatic rocks in the (a) Alxa Block (data from this study and Qin, 2012; Tang, 2015; Gong *et al.* 2018*a*; Zhang *et al.* 2018*d*; Liu *et al.* 2019; Pan, 2019; Song *et al.* 2019; Chen *et al.* 2020; Wang *et al.* 2020; Zhao *et al.* 2020) and (b) the southeastern Central Asian Orogenic Belt (data from Wang *et al.* 2015*b*).

the continued S-wards subduction of the PAO or by lithospheric extension. Accordingly, the tectonic setting of the Carboniferous magmatism in the northern margin of the NCC, either continental arc or lithospheric extension, can provide insights into the terminal evolutionary history of the southeastern CAOB.

The Alxa Block, also known as the Alxa Tectonic Belt (Song *et al.* 2018), connects the NCC to the east and the Tarim Craton to the west and lies between the CAOB to the north and the North Qilian Orogen to the south (Fig. 1a). Although this block is largely covered by deserts, numerous Phanerozoic plutons intruding into Precambrian metamorphic basement rocks crop out in its southwestern and northeastern parts (Fig. 1b). These plutons are mostly Palaeozoic in age, spanning Middle Ordovician–Early Devonian time (*c.* 458–394 Ma) and end Late Devonian–end Permian time (*c.* 359–252 Ma; Fig. 2a). Notably, this age pattern is quite similar to that of the southeastern CAOB (including the northern NCC), which includes two magmatic stages of middle Cambrian–Middle Devonian time (*c.* 508–386 Ma) and end Late Devonian–end Permian time (*c.* 362–252 Ma; Fig. 2b), indicating an operation of comparable

tectonic processes. Further, the early magmatic stage in the southwestern Alxa Block could also be related to the North Qilian Orogen (Duan *et al.* 2015; Zhang *et al.* 2017*a*; Wang *et al.* 2020), but the Qilian orogenesis ended before the Late Devonian Epoch (Xiao *et al.* 2009*a*; Song *et al.* 2013). The Carboniferous magmatism within the Alxa Block was therefore most likely related to the tectono-magmatic activity of the southeastern CAOB.

In this study, new geochronological, elemental and isotopic geochemical analyses of three early Carboniferous plutons in the southwestern Alxa Block are presented. These results, combined with regional correlations, suggest a lithospheric extensional setting rather than a simple continental arc for the development of early Carboniferous magmatism in both the Alxa Block and the southeastern CAOB.

2. Geological background

The Alxa Block is separated from the CAOB by the Enger Us Fault to the north, and from the North Qilian Orogen to the SW by the Longshoushan Fault (Fig. 1b). It is traditionally considered as the western part of the northern NCC (Fig. 1a), either the western part of the Yinshan Block (e.g. Zhao *et al.* 2005, 2012; Wan *et al.* 2006; Wang *et al.* 2016*b*, 2019*a*) or the western extension of the Khondalite Belt (e.g. Geng *et al.* 2010; Zhang *et al.* 2013*a*; Zhang & Gong, 2018). However, a close affinity of the Alxa Block to the Tarim or South China cratons had also been proposed (e.g. Tung *et al.* 2007; Yuan & Yang, 2015; Song *et al.* 2017), and the amalgamation of this block with the NCC might have taken place during early–middle Palaeozoic time (Dan *et al.* 2016; Zhang *et al.* 2016*c*), although no ophiolitic mélanges have been recognized between them until now. Nevertheless, in any of the proposed models, the Alxa Block has been considered as part of the northern NCC, having been amalgamated at least since the Carboniferous Period.

Three ophiolitic mélanges have been reported in Alxa area (Fig. 1b). Two of them crop out in the NE, including the *c.* 302 Ma Enger Us and the *c.* 275 Ma Quagan Qulu ophiolitic mélanges, with their basaltic rocks exhibiting normal mid-ocean-ridge basalt (N-MORB) and boninite-like geochemical features (Zheng *et al.* 2014), respectively. The Tepai ophiolitic mélange in the SW is also characterized by boninite-like basaltic rocks, but its formation age is either *c.* 278 Ma (Zheng *et al.* 2018) or *c.* 437–448 Ma (Pan, 2019).

The southwestern Alxa Block between the Longshoushan Fault and the Badain Jaran Desert involves the NW–SE-trending Beidashan and Longshoushan–Helishan mountains (Fig. 1c). The widespread Precambrian basement rocks in this area include the Neoarchean Beidashan complex (Gong *et al.* 2012; Zhang *et al.* 2013*a*) and Palaeoproterozoic Longshoushan Group (Tung *et al.* 2007; Gong *et al.* 2011). They consist of amphibolite- to greenschist-facies metamorphosed igneous and sedimentary rocks and are overlain unconformably by Neoproterozoic greenschist-facies meta-sedimentary rocks (Zhang & Gong, 2018). Recently, syenite of age *c.* 1.87 Ga and granitic gneiss of age *c.* 1.2 Ga were recognized in the Helishan area (Song *et al.* 2017; Wang *et al.* 2019*b*).

Lower Palaeozoic sedimentary rocks in the southwestern Alxa area crop out only to the south of the Longshoushan Fault (Fig. 1c). They are known as the Dahuangshan Formation and are composed of unmetamorphosed or greenschist-facies marine clastic and carbonate rocks (Zhang *et al.* 2016*a*). In contrast, the upper Carboniferous–middle Permian sedimentary rocks are widely
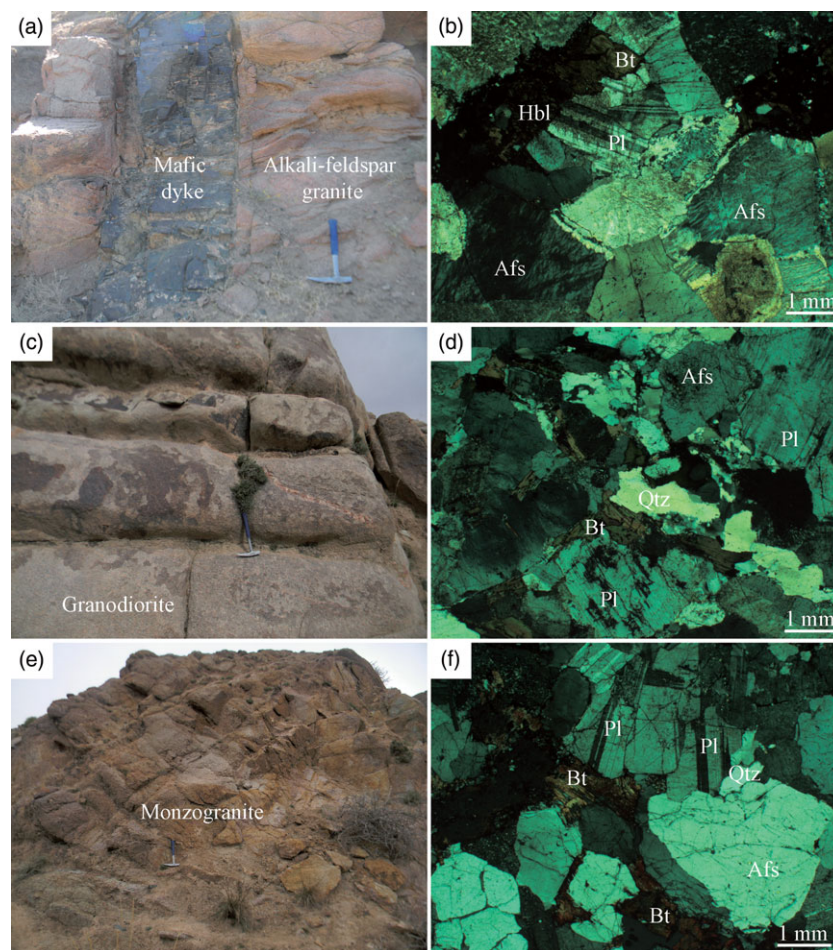
Fig. 3. (Colour online) Field photographs and mineral assemblages under microscope (cross-polarized light) of the studied late early Carboniferous plutons in the southwestern Alxa Block. (a, b) 17WAL-17, alkali-feldspar granite; (c, d) 17WAL-35, granodiorite; (e, f) 17WAL-39, monzogranite. Afs – alkali-feldspar; Bt – biotite; Hbl – hornblende; Pl – plagioclase; Qtz – quartz.

distributed (Fig. 1c). The upper Carboniferous succession consists of interbedded volcanic and clastic rocks in the lower part and shallow-marine bioclastic limestones and sandstones in the upper part, and is conformably overlain by lower–middle Permian strata, which include, from bottom to top, conglomerates, pebbly coarse sandstone, sandstone and siltstone, with volcanic interlayers. Mesozoic terrigenous clastic rocks are extensively distributed in this area (Fig. 1c).

Phanerozoic plutons are voluminous and widely exposed in the southwestern Alxa Block (Fig. 1c), with two magmatic periods of Middle Ordovician–Early Devonian and early Carboniferous–late Permian. Plutons of the earlier period are generally felsic granitoids (Qin, 2012; Wei *et al.* 2013; Tang, 2015; Liu *et al.* 2016b; Zhou *et al.* 2016; Zhang *et al.* 2018d; Wang *et al.* 2020), with only a few dolerite dykes (*c.* 424 Ma) in eastern Longshoushan (Duan *et al.* 2015). In contrast, plutons of the later period are widely distributed and include peridotite, gabbro, diorite, tonalite, granodiorite, monzogranite and granite (Chen *et al.* 2013; Jiao *et al.* 2017; Liu *et al.* 2017; Xue *et al.* 2017; Gong *et al.* 2018a, b; Huo, 2019; Song *et al.* 2019). In addition, several Triassic plutons crop out in the western Beidashan (Fig. 1c; Gu, 2012).

3. Samples and petrography

In this study, three granitic plutons were investigated and sampled in the southwestern Alxa Block; all are massive and salmon-pink to off-white in colour (Fig. 3). A medium- to coarse-grained alkali-feldspar granite in western Beidashan (17WAL-07; Fig. 1c) is composed of quartz (*c.* 30%), plagioclase (*c.* 20%), alkali-feldspar (*c.* 40%), biotite (*c.* 10%) and minor hornblende (Fig. 3b). The other two plutons are located in Longshoushan to the north of Shandan County (Fig. 1c). One is medium-grained granodiorite (17WAL-35) and composed of quartz (*c.* 20%), plagioclase (*c.* 40%), alkali-feldspar (*c.* 20%) and biotite (*c.* 20%; Fig. 3d). The other sample is coarse-grained monzogranite (17WAL-39), with similar mineral assemblage of quartz (*c.* 25%), plagioclase (*c.* 25%), alkali-feldspar (*c.* 30%) and biotite (20%; Fig. 3f). Accessory minerals of zircon, apatite and titanite are present in all three plutons.

4. Analytical methods

4.a. Whole-rock major- and trace-element analyses

Fresh granitoid samples were first crushed and then ground to 200 mesh in a tungsten carbide cup and ball mill, and then analysed geochemically at the National Research Center of Geoanalysis, China Geological Survey. Whole-rock major-element oxides were measured using a Malvern Panalytical Axios PW4400 x-ray fluorescence spectrometer (XRF), and the analytical uncertainties are generally between 1% and 5%. The concentrations of trace and rare earth elements were determined by a PerkinElmer NexION 300Q inductively coupled plasma mass spectrometer (ICP-MS), with analytical precision generally better than 5%.
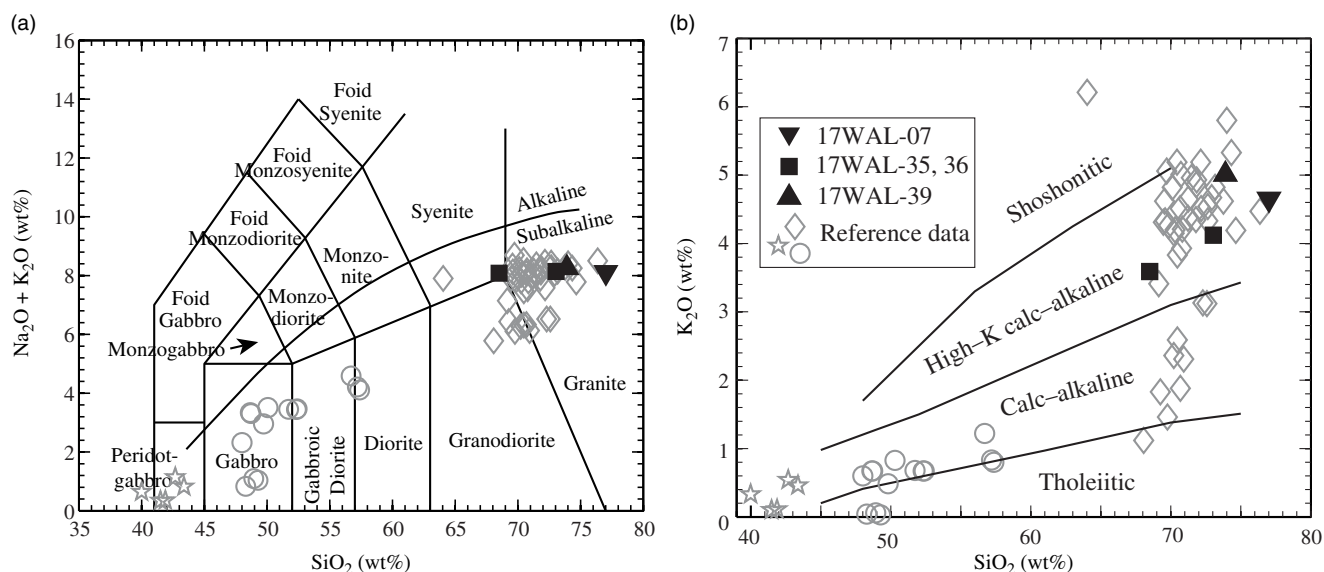
Fig. 4. (a) $Na_2O + K_2O$ versus SiO_2 and (b) K_2O versus SiO_2 diagrams for the early Carboniferous plutons in the Alxa Block. Data sources include Wang *et al.* (2015*b*), Dan *et al.* (2016), Liu *et al.* (2016*a*) and Xue *et al.* (2017).

4.b. Zircon U–Pb dating

Zircon grains were firstly separated by conventional heavy liquid and magnetic techniques, and then hand-picked under a binocular microscope. The selected zircon crystals were mounted in epoxy resin and polished to half thickness. Potential analytical spots were determined based on morphological features and internal structures of zircons on optical and cathodoluminescence (CL) images. Zircon U–Pb analyses on mineral separates from the three samples were conducted in Tianjin Institute of Geology and Mineral Resources, China Geological Survey, China. A Thermo Fisher Scientific multi-collector inductively coupled plasma mass spectrometer (MC-ICP-MS; Neptune) was coupled to a New Wave 193 nm ArF excimer laser ablation system. Detailed procedures are reported by Cui *et al.* (2012). Zircon standard GJ-1 was employed as an external standard (Jackson *et al.* 2004), and measurements of zircon standard Plešovice, which was used as an unknown, yielded a weighted mean $^{206}Pb/^{238}U$ age of 335.5 ± 2.6 Ma (*n* = 12; 2σ). This result is in good agreement with the recommended value within error (337.13 ± 0.37 Ma; Sláma *et al.* 2008). The corrections of common lead were carried out using the method of Andersen (2002). Concordia diagrams and ages were obtained using ISOPLOT 4.15 (Ludwig, 2012). Uncertainties of individual measurements were at the 1σ level, but the weighted mean ages and concordia diagrams were given at the 2σ level (95% confidence level).

4.c. Sr–Nd isotopic analyses

The whole-rock Sr and Nd isotopic compositions were determined using a Finnigan MAT-262 mass spectrometer and a Nu Plasma high-resolution MC-ICP-MS, respectively, at the Institute of Geology, Chinese Academy of Geological Sciences, China. The measured $^{87}Sr/^{86}Sr$ ratio of the $SrCO_3$ standard SRM 987 was 0.710243 ± 0.000012 (2σ), in good agreement with the recommended value within error (0.710251 ± 0.000018; Coombs *et al.* 2004). Two standards of JMC Nd_2O_3 (reference value = 0.511137 ± 0.000008; Jahn *et al.* 1980) and GSB 04-3258-2015 (certified value = 0.512438; Tang *et al.* 2017) were employed during Nd isotopic analyses, with measured $^{143}Nd/^{144}Nd$ ratios of

0.511123 ± 0.000010 and 0.512441 ± 0.000012 at the 2σ level, respectively. Detailed analytical procedures for both Sr and Nd isotopic compositions are described by Tang *et al.* (2021). All measured ratios were corrected for mass fractionation by normalizing to $^{88}Sr/^{86}Sr = 8.37521$ and $^{146}Nd/^{144}Nd = 0.7219$, respectively.

5. Results

Whole-rock major- and trace-element concentrations, LA-ICP-MS zircon U–Pb data and Sr–Nd isotopic compositions are given in online Supplementary Tables S1–S3 (available at http://journals.cambridge.org/geo), respectively.

5.a. Whole-rock major and trace elements

All three plutons have high SiO_2 (68.49–77.01 wt%) and $K_2O + Na_2O$ (8.07–8.25 wt%; Fig. 4a) and low MgO (0.17–0.82 wt%) and MnO (0.03–0.06 wt%), show peraluminous features (A/CNK = 1.04–1.13), and belong to the high-K calc-alkaline series (Fig. 4b). Alkali-feldspar granite 17WAL-07 and monzogranite 17WAL-39 display lower CaO (0.59–0.61 wt%), higher K_2O ($K_2O/Na_2O = 1.35$–1.55), higher total rare earth element (REE) concentrations (257.58–275.96 ppm) and distinct negative Eu anomalies (δEu = 0.17–0.37; Fig. 5a), with enrichments in large-ion-lithophile elements (LILEs; e.g. Cs, Rb, Th and Pb) and depletions in Nb, Ta, Ba and Sr (Fig. 5b). In comparison, granodiorite 17WAL-35 displays relatively higher CaO (1.52–2.51 wt%) and lower total REE concentrations (114.30–206.16 ppm), with significantly enriched light rare earth elements (LREEs; $(La/Yb)_N = 35.75$–56.24) and positive Eu anomalies (δEu = 1.12–1.14; Fig. 5c). Moreover, it is characterized by enriched LILEs (Cs, Rb, Ba, Th, Pb and Sr) and depleted high-field-strength elements (HFSEs; Y, Yb and Lu), with negative Nb–Ta and positive Zr–Hf anomalies, respectively (Fig. 5d).

5.b. Zircon U–Pb ages

Zircon grains from the studied samples are transparent, euhedral and short columnar or prismatic in shape. They exhibit well
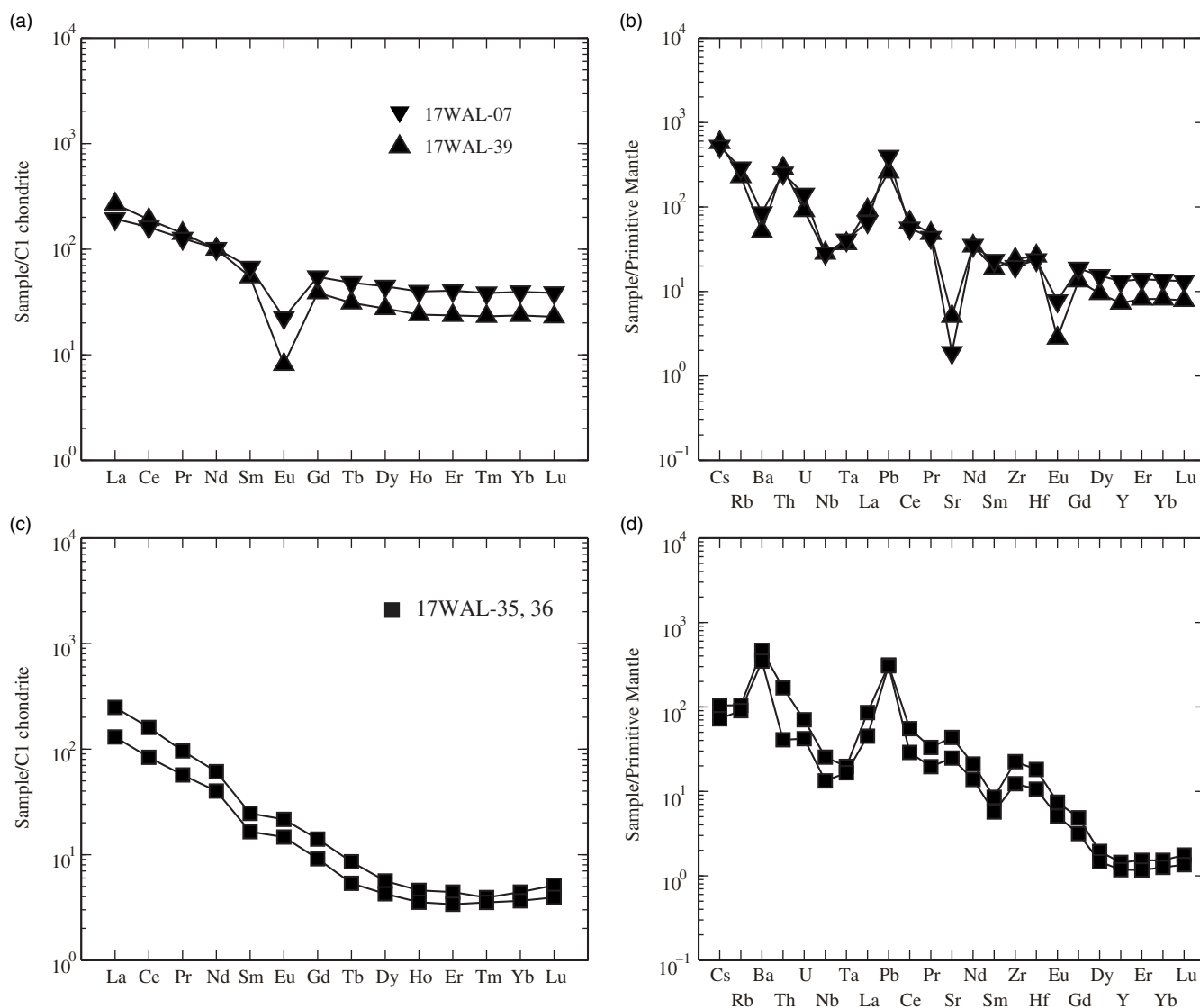
Fig. 5. (a, c) Chondrite-normalized REE patterns and (b, d) primitive mantle-normalized trace-element diagrams for the late early Carboniferous plutons in the southwestern Alxa Block. Compositions of C1 chondrite and primitive mantle after Sun & McDonough (1989).

preserved concentric magmatic oscillatory zoning, with a few inherited zircon cores appearing occasionally in samples 17WAL-35 and 39 (Fig. 6). For alkali-feldspar granite 17WAL-07, all 24 spots are concordant and cluster together (Fig. 7a). Their Th/U ratios are 0.33–0.51 and they yield a concordia age of 331.6 ± 1.6 Ma (mean square weighted deviation (MSWD) = 4.2; 2σ, decay-constant errors included), which is consistent with the weighted mean ^{206}Pb/^{238}U age (331.7 ± 1.5 Ma; MSWD = 1.01; 2σ). With the exception of four discordant spots (16, 17, 18 and 22), concordant analyses of the other 21 granodiorite 17WAL-35 spots have Th/U ratios of 0.36–0.83 but form two age clusters (Fig. 7b). The older population includes 17 spots with a weighted mean ^{206}Pb/^{238}U age of 344.1 ± 2.2 Ma (MSWD = 1.40; 2σ; Fig. 7b1) and the younger population includes 4 spots with a weighted mean ^{206}Pb/^{238}U age of 326.2 ± 6.6 Ma (MSWD = 1.50; 2σ; Fig. 7b2). Furthermore, monzogranite 17WAL-39 has six discordant spots (1, 8, 11, 16, 17 and 21) and one concordant age cluster (Fig. 7c), which yields a consistent concordia age of 331.8 ± 1.7 Ma (MSWD = 4.8; 2σ, decay-constant errors included) and weighted mean ^{206}Pb/^{238}U age of

331.9 ± 1.7 Ma (MSWD = 0.88; *n* = 17; 2σ), with Th/U ratios of 0.43–1.03.

5.c. Whole-rock Sr–Nd isotopes

The ^{87}Rb/^{86}Sr and ^{147}Sm/^{144}Nd ratios of three granitic samples were calculated using the measured whole-rock Rb, Sr, Sm and Nd concentrations. The alkali-feldspar granite (17WAL-07; *t* = 332 Ma) has the lowest initial ^{87}Sr/^{86}Sr (0.700128) and highest initial ^{143}Nd/^{144}Nd (0.512219) ratios among the three plutons, with positive $\epsilon_{Nd}(t)$ value (0.16) and Mesoproterozoic Nd model age (T_{DM} = 1207 Ma; Fig. 8). The initial ^{87}Sr/^{86}Sr ratio of the granodiorite (17WAL-35; *t* = 326 Ma) is low (0.705102), and its initial ^{143}Nd/^{144}Nd ratio and $\epsilon_{Nd}(t)$ value are 0.511358 and −16.80, respectively (Fig. 8). As its $f_{Sm/Nd}$ (−0.59) significantly deviates from that of the average crust (−0.40; DePaolo *et al.* 1991), both T_{DM} (1847 Ma) and T_{DM2} (2446 Ma) were calculated. For the monzogranite (17WAL-39; *t* = 332 Ma), its initial ^{87}Sr/^{86}Sr and ^{143}Nd/^{144}Nd ratios are 0.717670 and 0.511706, respectively, with negative $\epsilon_{Nd}(t)$ value (−9.85) and Palaeoproterozoic T_{DM2} (1889 Ma; Fig. 8).
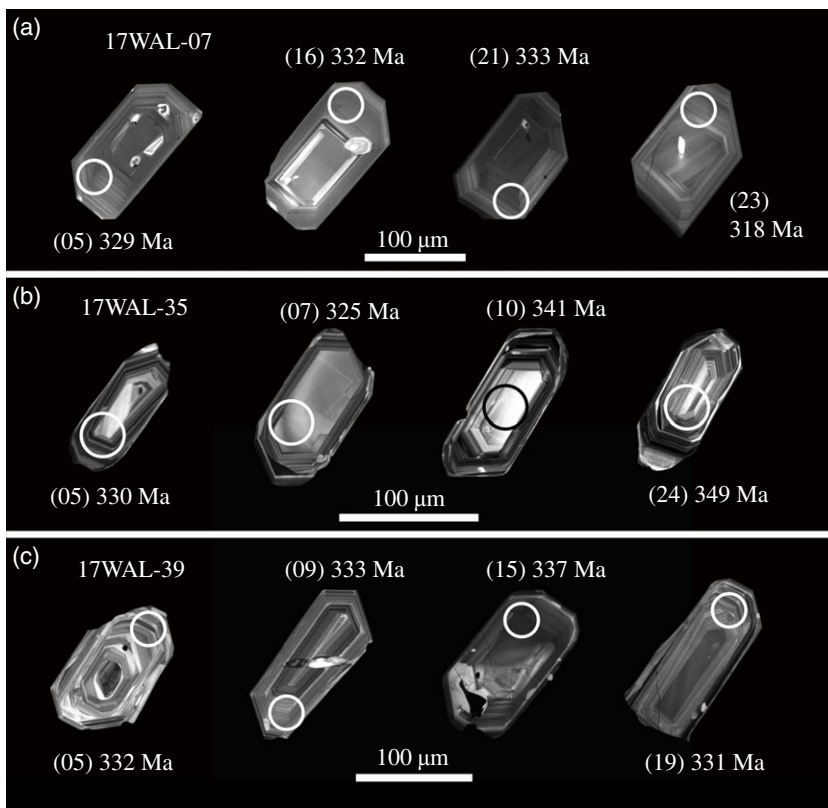
Fig. 6. Cathodoluminescence (CL) images of representative zircon grains from the studied late early Carboniferous plutons in the southwestern Alxa Block.

6. Discussion

The well preserved concentric magmatic oscillatory zoning (Fig. 6) and high Th/U ratios (0.33–1.03) of dated zircon grains indicate their magmatic origin (Corfu et al. 2003); the concordia and weighted mean $^{206}Pb/^{238}U$ ages are therefore interpreted as crystallization ages (Fig. 7). Because several spots from the older age cluster of granodiorite (17WAL-35) are located within the inherited zircon cores (e.g. spot 24 in Fig. 6b), the younger age cluster is employed. The three granitic plutons in the southwestern Alxa Block were therefore formed during late early Carboniferous time (c. 332–326 Ma).

6.a. Petrogenesis of the studied late early Carboniferous granitic plutons

The alkali-feldspar granite (17WAL-07) and monzogranite (17WAL-39) have similar geochemical features, such as high $K_2O + Na_2O$ (8.10–8.25 wt%), FeO^T (1.49–1.51 wt%) and FeO^T/MgO (4.38–8.87), low CaO (0.59–0.61 wt%), MgO (0.17–0.43 wt%) and P_2O_5 (< 0.06 wt%), high total REE concentrations (257.58–275.96 ppm) with V-type REE patterns (Fig. 5a), and strongly depleted Ba and Sr (Fig. 5b). These characteristics indicate A-type granite nature, which can be clearly identified on the discrimination diagrams (e.g. Fig. 9b, c; Whalen et al. 1987; King et al. 1997). A-type granites may originate from the fractionation of mantle-derived basaltic magmas (Eby, 1990, 1992; Bonin, 2007), the mixing of mantle- and crust-derived magmas (Yang et al. 2006), or the partial melting of crust at high temperatures (Whalen et al. 1987; King et al. 1997; Wu et al. 2002). If rhyolitic magmas were derived from fractional crystallization of coeval basaltic magmas, the two components would commonly be spatially and temporally associated (Whitaker et al. 2008). If the plutons had their origin by magma mixing, then they would have

intermediate compositions with the presence of profuse mafic microgranular enclaves (MMEs; Yang et al. 2006, 2007; Zhang et al. 2016b), although the MMEs may be also cogenetic with their host granitoids (Zhang & Zhao, 2017). The two A-type granites in the southwestern Alxa Block are rhyolitic in composition (Fig. 4a), but no MMEs were observed (Fig. 3a, e) and their coeval mafic intrusions crop out far away in the northeastern Alxa Block (Wang et al. 2015b; Liu et al. 2016a). They are also characterized by high SiO_2 (73.89–77.01 wt%) and K_2O/Na_2O (1.35–1.55) and are peraluminous (A/CNK = 1.04–1.13), similar to aluminous A-type granites with continental crustal sources (King et al. 1997). Moreover, the alkali-feldspar granite has low positive $\epsilon_{Nd}(t)$ value (0.16) and Mesoproterozoic Nd model age (1207 Ma; Fig. 8b), which is close to the protolith crystallization age of a granitic gneiss in the Helishan (c. 1200 Ma; Song et al. 2017). Its unusually low initial $^{87}Sr/^{86}Sr$ value (0.700128; Fig. 8a) may be caused by the strong depletion of Sr (Fig. 5b), as the initial $^{87}Sr/^{86}Sr$ value was calculated based on the measured whole-rock Sr concentration. The monzogranite has radiogenic Sr–Nd isotopes (Fig. 8a) and a Palaeoproterozoic Nd model age (1889 Ma; Fig. 8b). The Palaeoproterozoic basement rocks are commonly observed in Longshoushan (Tung et al. 2007; Gong et al. 2011), in addition to a c. 1872 Ma syenite in Helishan (Wang et al. 2019b). The two aluminous A-type granites were therefore most probably the high-temperature partial melts of Palaeo- and Mesoproterozoic crustal materials.

The granodiorite (17WAL-35) is also high-K calc-alkaline (Fig. 4b) and weakly peraluminous (A/CNK = 1.07–1.08) and has depleted HREEs and HFSEs (Fig. 5c, d). It is chemically characterized by high Sr (522.0–918.0 ppm) and low Y (5.36–6.56 ppm) and Yb (0.62–0.75 ppm) concentrations, with high Sr/Y ratios (97.4–139.9). Although high Sr/Y ratio (> 40) usually occurs in adakitic rocks, the high K_2O contents (3.59–4.12 wt%) and
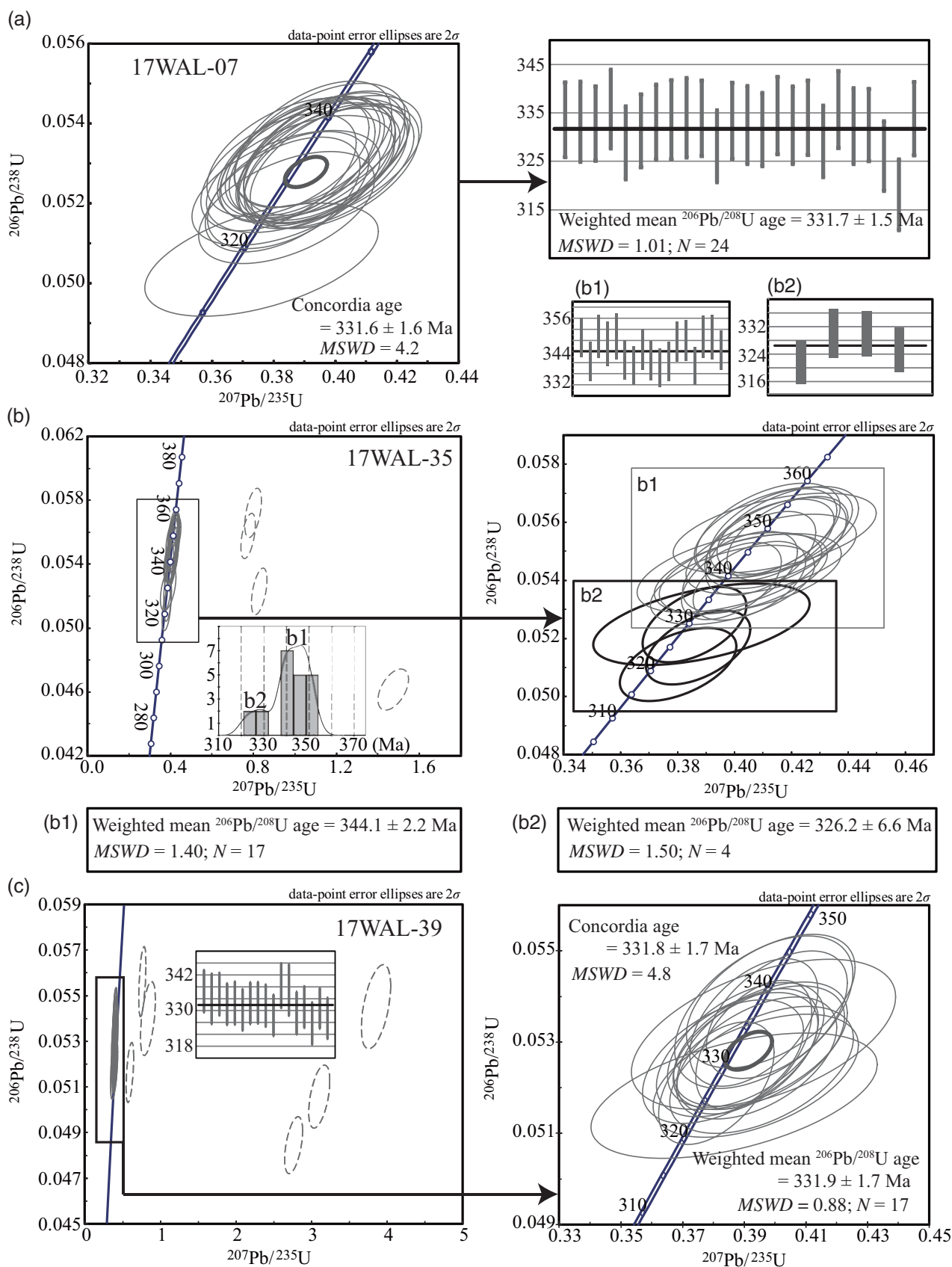
Fig. 7. (a–c) Concordia diagrams showing LA-ICP-MS zircon U–Pb data of the studied late early Carboniferous plutons in the southwestern Alxa Block (all the diagrams and calculations are at the 2σ level).
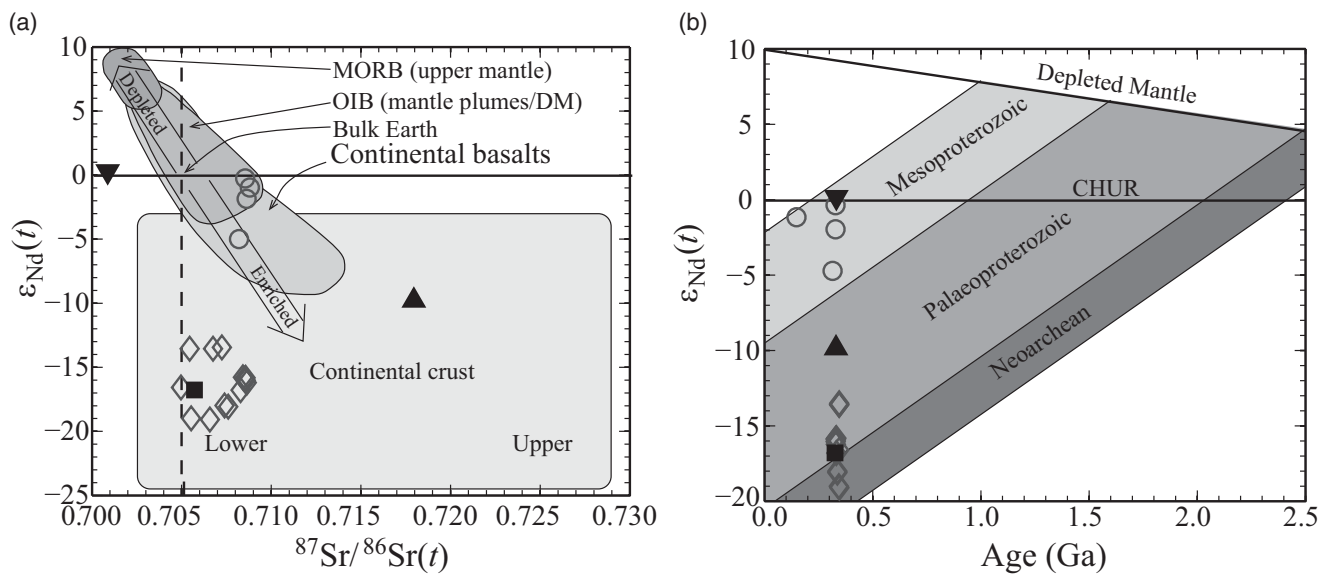
Fig. 8. Sr–Nd isotopic features of early Carboniferous plutons in the Alxa Block. Symbols and data sources as for Figure 4.

K_2O/Na_2O ratios (0.80–1.03) of this granodiorite are more 'continental' than typical adakites (Defant & Drummond, 1990; Martin *et al.* 2005; Moyen, 2009). The coexistence of negative Nb–Ta and positive Zr–Hf anomalies (Fig. 5d) and highly radiogenic Sr–Nd isotopes (Fig. 8a) also suggest a continental crustal source (Rudnick & Gao, 2003). The enrichments of Eu, Ba and Sr are attributed to the large proportion of plagioclase (*c.* 40%), whereas the low Y concentration may suggest the presence of garnet in the residue, so that the high Sr/Y ratios indicate a deeper crustal level of magma source (Ducea *et al.* 2015). In addition, *c.* 2.5 Ga basement rocks and magmatic activity are commonly observed in the southwestern Alxa Block (Zhang *et al.* 2013a; Zhang & Gong, 2018; Wang *et al.* 2019b), which is coeval with the two-stage Nd model age of this granodiorite (*c.* 2446 Ma; Fig. 8b). This granodiorite of high Sr/Y ratio may therefore have its origin in the partial melting of upper Neoarchean lower crust.

6.b. Tectonic setting of the early Carboniferous magmatism in the Alxa Block

Two different tectonic processes accounting for the early Carboniferous magmatism within the Alxa Block were proposed previously: continental arc magmatism induced by the S-wards subduction of the PAO (Liu *et al.* 2016a; Xue *et al.* 2017; Gong *et al.* 2018a), or the collision and amalgamation between the Alxa Block and the NCC (Zhang *et al.* 2013b; Dan *et al.* 2016). Noticeably, whether a Palaeozoic suture between the Alxa Block and the NCC existed or not is still in debate, especially with no associated ophiolitic mélanges observed (e.g. Dan *et al.* 2016; Zhang & Gong, 2018; Wang *et al.* 2019b), and the early Carboniferous magmatic rocks are widely distributed, rather than along a linear trend in the eastern margin of the Alxa Block (Fig. 1b), so they are less likely attributed to such an amalgamation process. Furthermore, the argument of continental arc magmatism is mainly based on their arc-like geochemical signatures, such as calc–alkaline characteristics (Fig. 4b), negative Nb–Ta anomalies and high Sr/Y ratios (e.g. Liu *et al.* 2016a; Xue *et al.* 2017). However, these signatures can also be inherited from magma sources (Wang *et al.* 2016a), and most granites of high Sr/Y ratio

in this area exhibit high K_2O/Na_2O ratios (0.92–3.70), positive Zr–Hf anomalies and radiogenic Nd–Hf isotopes, indicating derivation by the partial melting of lower continental crust (Fig. 8a; Dan *et al.* 2016; Xue *et al.* 2017); this can occur not only in continental arc belts but also in lithospheric extensional environments.

It is noteworthy that the early Carboniferous plutons within the Alxa Block are mostly basic or acidic in silica content (Fig. 4), resembling bimodal associations. The felsic plutons plot not only in volcanic arc but also in within-plate and post-collision granite fields (Fig. 9a), with most of them exhibiting radiogenic Sr–Nd isotopes (Fig. 8a). They are characterized by the coexistence of A-type granites, peraluminous granites and calc-alkaline I-type granitoids (Dan *et al.* 2016; Liu *et al.* 2016a; Xue *et al.* 2017; Zheng *et al.* 2019), which mostly occur in extensional settings (Maniar & Piccoli, 1989). A-type granites usually indicate high-temperature anatectic conditions related to asthenospheric upwelling in a lithospheric extensional setting (Whalen *et al.* 1987; Eby, 1992). The mafic plutons plot mostly in the MORB and within-plate basalt fields, similar to the rift-related Basin-and-Range basalts (Fig. 10), and display juvenile or weakly radiogenic Sr–Nd isotopes (Fig. 8a). It is noteworthy that several of the mafic plutons in the northeastern Alxa Block have horn-blende as the dominant mafic mineral and resemble appinitic intrusions in geochemistry (Wang *et al.* 2015b). Generally, mafic appinitic melts were most likely produced by the partial melting of subduction-modified sub-continental lithospheric mantle (Fig. 10c) and the melting may be triggered by asthenospheric upwelling following slab break-off or delamination after a subduction event (Murphy, 2013). The generation of both the mafic and felsic early Carboniferous plutons within the Alxa Block therefore most likely resulted from the asthenospheric upwelling at that time. Although an upwelling asthenosphere may also occur in a continental arc setting, continental arc magmatism is typically characterized by linear tracks within a specific tectonic unit and dominated by andesitic rocks, with continued major elemental compositions from basalts to rhyolites but without compositional gaps (Ducea *et al.* 2015). Evidently, this is not the case for the early Carboniferous plutons within the Alxa Block (Figs 1b, 4a),
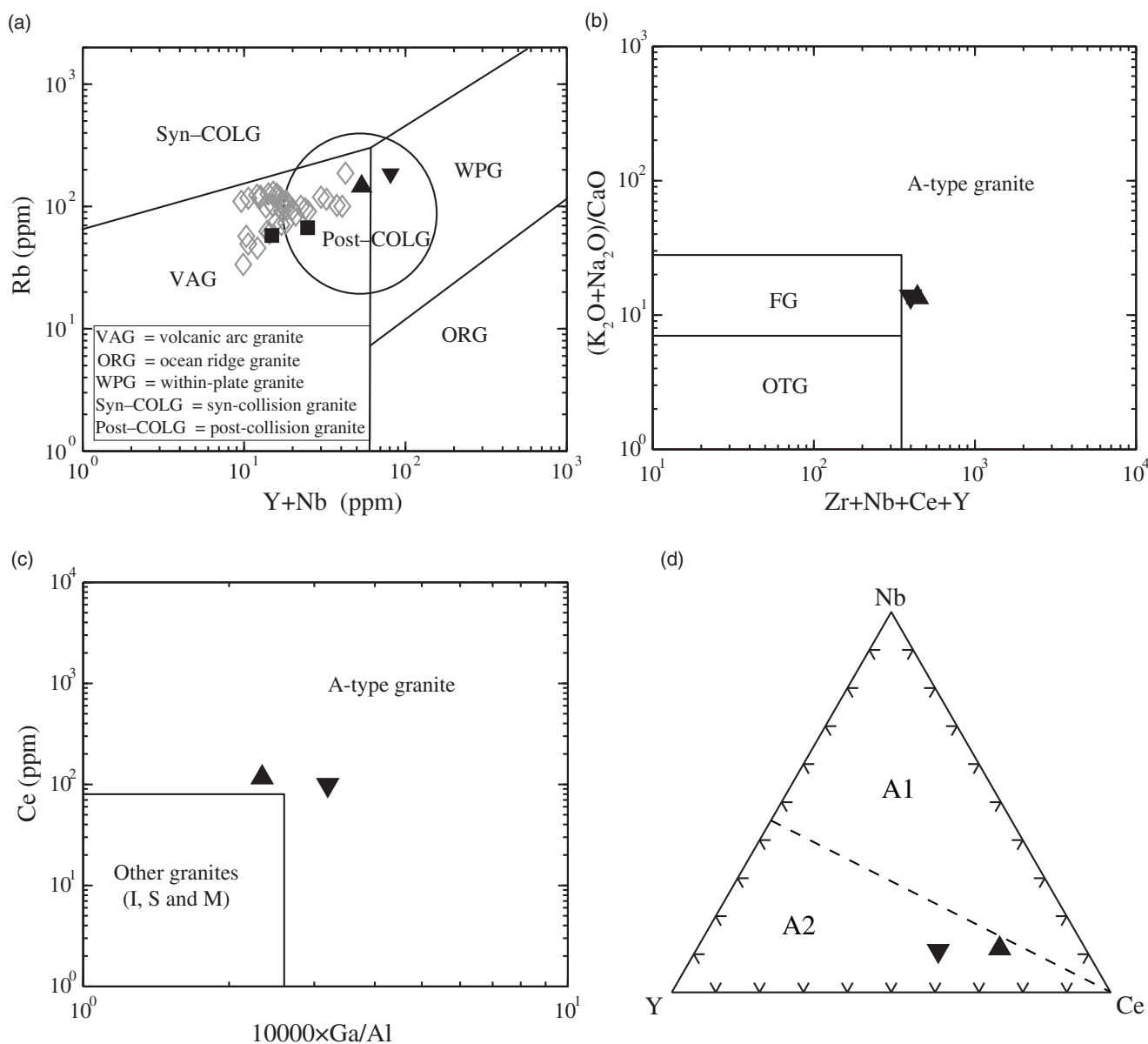
Fig. 9. (a) Tectonic discrimination diagrams of Rb versus (Y + Nb) for the early Carboniferous felsic plutons in the Alxa Block (Pearce, 1996). (b) Plot of (K$_2$O + Na$_2$O)/CaO versus Zr + Nb + Ce + Y and (c) plot of Ce versus 10 000×Ga/Al for A-type granites (Whalen *et al.* 1987). (d) Nb–Y–Ce diagram for distinguishing between A1 and A2 granites (Eby, 1992). Symbols and data sources as for Figure 4.

meaning that their formation in a continental arc is less likely, but rather more likely in a lithospheric extensional setting.

Furthermore, A-type granites are a good indicator of lithospheric extension, but the specific extensional setting could be varied (Sain *et al.* 2017), including not only rift-related (intraplate) extension (Whalen *et al.* 1987; Eby, 1992) but also back-arc extension (Karsli et al. 2012; Bickford *et al.* 2015). The two early Carboniferous aluminous A-type granites in the southwestern Alxa Block are A2 type (Fig. 9d) and therefore represent magmas derived from continental crust that has been through an orogenic cycle of arc magmatism and collision (Eby, 1992). The geochemical similarities between early Carboniferous mafic plutons in the Alxa Block and Basin-and-Range basalts (Fig. 10), which were generated in back-arc extensional setting to the Sierra Nevada arc (Cousens *et al.* 2019), also suggest a subduction-related tectonic setting. In back-arc extensional setting, the asthenospheric upwelling could

be induced by the foundering of arc root during the roll-back process of subducting slab (DeCelles *et al.* 2009; DeCelles & Graham, 2015). Another possibility is the intra-continental extensional setting, because the sub-continental lithospheric mantle and lower continental crust of the Alxa Block had been modified by subduction during Middle Ordovician–Early Devonian time (Liu *et al.* 2016b; Zhou *et al.* 2016), and the subduction-related geochemical signatures of later magmas may be inherited from the subduction-modified magma sources (Wang *et al.* 2016a). Moreover, the extension-related rock associations of calc-alkaline I-type granites, aluminous A2-type granites and peralkaline granites were present in the southwestern Alxa Block from late Silurian–Early Devonian time, following earlier arc magmatism and implying post-collisional setting (Wang *et al.* 2020). In addition, the cyclical magmatic flare-ups and lulls within each Palaeozoic magmatic stage of the Alxa Block (Fig. 2a) are quite
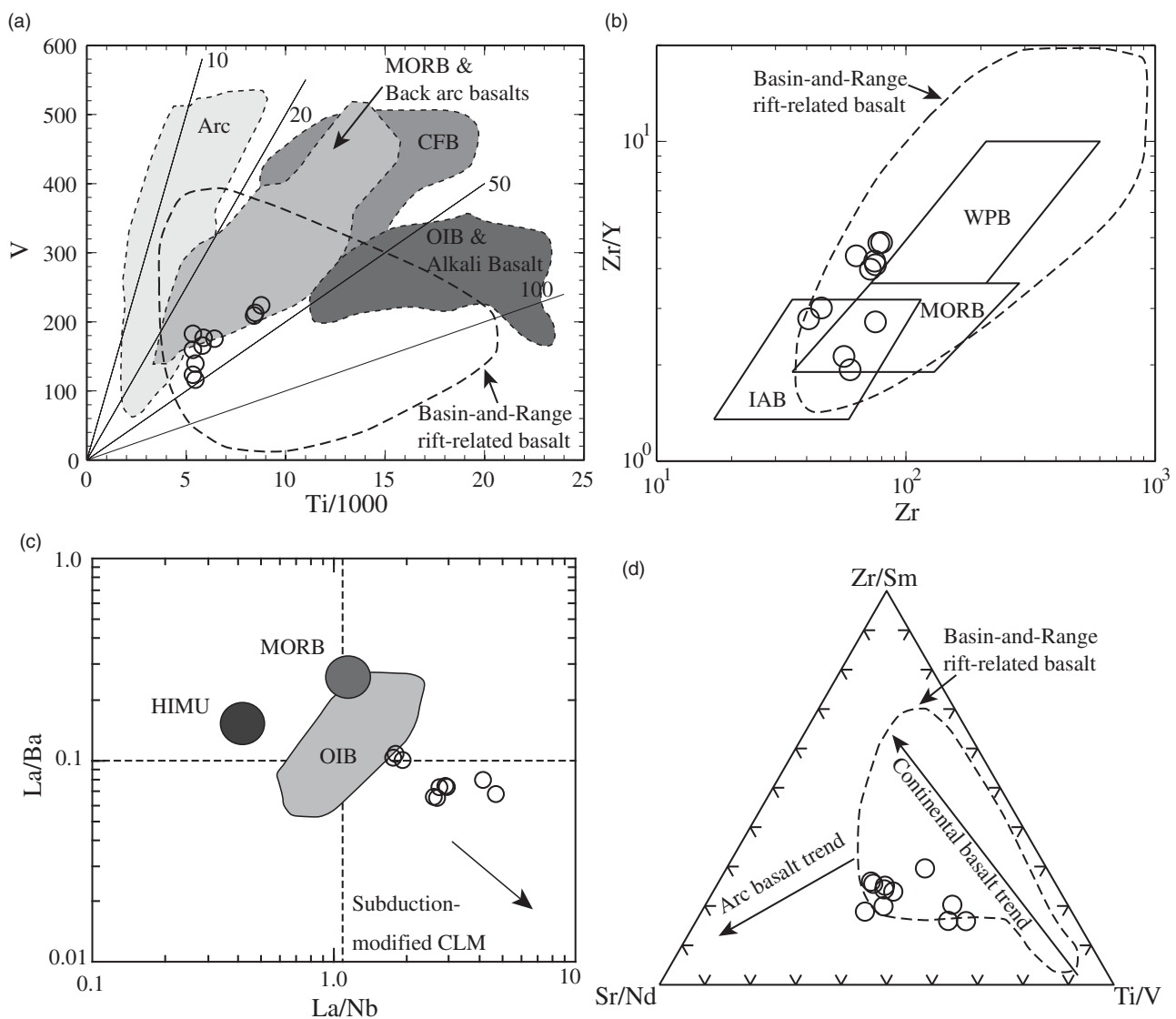
Fig. 10. Petrogenetic discrimination diagrams of (a) V–(Ti/1000) (Shervais, 1982), (b) (Zr/Y)–Zr (Pearce & Norry, 1979), (c) (La/Ba)–(La/Nb) (Saunders *et al.* 1992), and (d) (Zr/Sm)–(Sr/Nd)–(Ti/V) (Wang *et al.* 2016a) for the early Carboniferous mafic rocks in the Alxa Block. The Basin-and-Range rift-related basalt field refers to Wang *et al.* (2016a). Symbols and data sources as for Figure 4.

similar to those of Cordilleran arcs in terms of time span and frequency (DeCelles *et al.* 2009), but the magmatic hiatus between the two magmatic stages is relatively too long for one single subduction event. The two magmatic stages of the Alxa Block may therefore represent two orogenic cycles and the early Carboniferous extension, as the initiation of the second orogenic cycle, may suggest intra-continental extensional setting. Although more geological evidence is urgently needed to discriminate between the two kinds of extensional settings, a simple continental arc model is less likely for the early Carboniferous magmatism within the Alxa Block.

Additionally, continental arc magmatism is usually accompanied by syn-arc sedimentation in fore-arc or back-arc basins (Ducea *et al.* 2015), but lower Carboniferous strata are absent from the Alxa Block based on available geological reports. Although a few outcrops in the northern Alxa Block were previously identified as lower Carboniferous deposits, they were recently reassigned as lower–middle Permian strata (Zhang *et al.* 2018c). By contrast, the upper Carboniferous–middle Permian strata are widely distributed. The sedimentary facies show a distinct change from terrestrial alluvial fan and delta in the lower stratigraphic sections to platform, littoral and shallow-marine in the upper stratigraphic sections, with abundant fossils (e.g. plants, fusulinids, brachiopods, corals) and volcanic interlayers (Bu *et al.* 2012; Han *et al.* 2012; Yin *et al.* 2016; Song *et al.* 2018). Such a transgression sequence is consistent with the further development of the lithospheric extension.

6.c. Tectonic implications for the development of southeastern CAOB

Even if the Alxa Block was separated from the NCC during the Precambrian Eon, sedimentologic, magmatic and structural evidences (Li *et al.* 2012a; Dan *et al.* 2016; Zhang *et al.* 2013b, 2016c) all suggest that their amalgamation occurred before early Carboniferous time. Palaeomagnetic studies also suggest that the Precambrian micro-continental blocks within the southeastern CAOB (e.g. Mongolia, Songliao and Hunshandake blocks) may
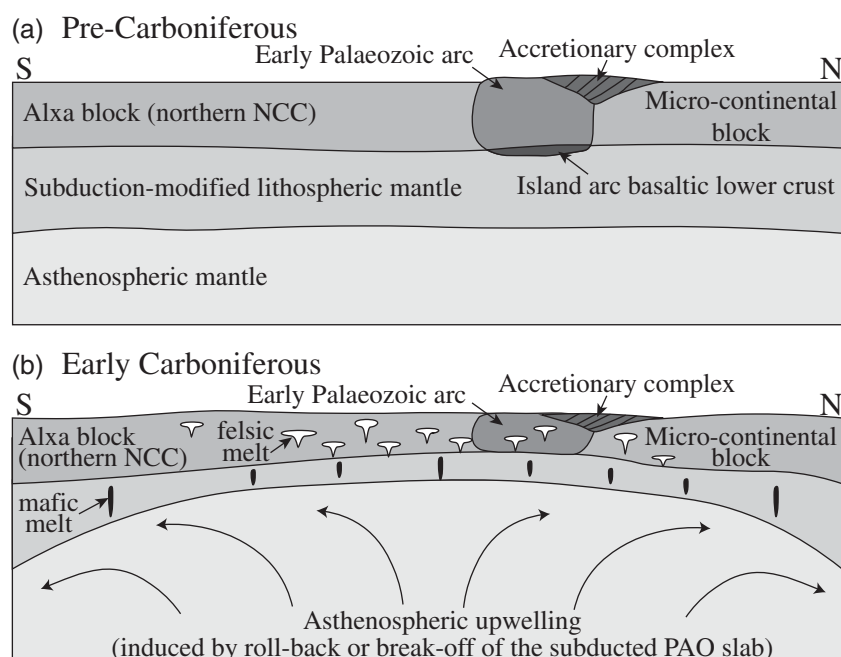
Fig. 11. Extensional tectonics of the Alxa Block and the southeastern CAOB during early Carboniferous time. (a) Micro-continental blocks within the southeastern CAOB had already been accreted to the northern NCC (Alxa Block) before early Carboniferous time. (b) During early Carboniferous time, the asthenospheric upwelling induced by either the roll-back or the break-off of the subducted PAO slab heated both the subduction-modified lithospheric mantle and the overlying crust, leading to the generation of the mafic and felsic plutons, respectively.

have already accreted to the northern NCC by early Carboniferous time (Pruner, 1992; Li *et al.* 2012*b*; Zhao *et al.* 2013; Zhang *et al.* 2018*a*). Furthermore, the Palaeozoic magmatic episodes of the Alxa Block and the southeastern CAOB (including the northern margin of the NCC) are very similar (Fig. 2), indicating comparable tectonic processes. Consequently, the whole region had been experiencing a uniform tectonic regime since early Carboniferous time and, if there was on-going S-wards subduction of the large-scale PAO at that time, the arc-trench system was most likely located to the north of these micro-continental blocks.

Regionally, the early Carboniferous is the initial period of the second magmatic stage (Fig. 2), and magmatic rocks during this period are characterized by the mafic–ultramafic complexes in northern Inner Mongolia (Jian *et al.* 2012; Zhang *et al.* 2015*c*; Li *et al.* 2018), the appinitic intrusions in the northern NCC (Zhou *et al.* 2009; Zhang *et al.* 2012*a*; Wang *et al.* 2015*b*), the calc-alkaline I-type and peraluminous granites with crustal origins throughout the southeastern CAOB (Bao *et al.* 2007; Zhang *et al.* 2007, 2011; Liu *et al.* 2009, 2016*a*; Blight *et al.* 2010; Dan *et al.* 2012; Xue *et al.* 2017), and the A-type granites newly identified in the southwestern Alxa Block (this study). Such rock associations are commonly associated with asthenospheric upwelling in lithospheric extensional setting. Although some of the basaltic rocks from the mafic–ultramafic complexes exhibit subduction-related geochemical features (Jian *et al.* 2012; Zhang *et al.* 2015*c*; Li *et al.* 2018), these features can also be imprinted by crustal contamination (Xia, 2014) or inherited from magma sources that have been modified by earlier subduction fluids or melts (Wang *et al.* 2016*a*). Further, the coeval intrusions are widely distributed (Xu *et al.* 2014) rather than along one or two specific ribbons as would be expected for a magmatic arc, supporting their formation in an extensional tectonic setting. Moreover, if this lithospheric extension occurred in back-arc, then the remnants of the large-scale PAO may be represented by the early Carboniferous Erenhot–Hegenshan ophiolitic mélanges to

the north of the micro-continental blocks (Zhang *et al.* 2015*c*; Li *et al.* 2018). Otherwise, the early Carboniferous extension of the southeastern CAOB was probably developed in an intra-continent environment and may represent the initiation of the second orogenic cycle (Xu *et al.* 2018).

In addition to the intrusions, the early Carboniferous sedimentary rocks are mostly absent from the southeastern CAOB, indicating regional uplift related to asthenospheric upwelling during the initial stage of the lithospheric extension. The Carboniferous metamorphic rocks are high-temperature–low-pressure and show a clockwise *P–T* path, involving pre-peak heating with slight decompression, peak and post-peak cooling stages, also suggesting an extension process (Zhang *et al.* 2018*b*).

Subsequently, the late Carboniferous–Permian magmatism in the southeastern CAOB became intense (Fig. 2) with the formation of the widespread bimodal volcanic rocks, continental basaltic intrusions, calc-alkaline I-type granites, peraluminous S-type granites, A-type granites and several peralkaline magmatic belts (e.g. Jahn *et al.* 2009; Zhang *et al.* 2012*b*, 2015*b*, 2016*d*, 2017*b*; Pang *et al.* 2016, 2017; Zhao *et al.* 2016*a*; Ji *et al.* 2018; Wang *et al.* 2021*b*), implying further development of the early Carboniferous extension. This is also consistent with the occurrence of many late Carboniferous–Permian mafic dykes (Fig. 3a) with MORB or within-plate basalt geochemical signatures in this region (Lin *et al.* 2014). Accordingly, the late Carboniferous–Permian Solonker, Enger Us and Quagan Qulu ophiolitic mélanges (Jian *et al.* 2010; Zheng *et al.* 2014), which contain MORB-type intrusions, continental basalts and terrigenous sediments (Luo *et al.* 2016; Shi *et al.* 2016), may represent the newly opened limited ocean basins and mark the strongest extension (Xu *et al.* 2014, 2018). The late Carboniferous–Permian sedimentary sequences are also widely exposed throughout the southeastern CAOB. They vary from plant fossil-bearing terrigenous clastic rocks to shallow-marine clastic and carbonate

depositions, with basal conglomerates, and are transgression sequences related to regional extension (Zhao *et al.* 2016b; Ji *et al.* 2020; Wang *et al.* 2021a).

To summarize, we propose a lithospheric extensional process rather than a simple continental arc for the tectono-magmatic development of the southeastern CAOB during early Carboniferous time (Fig. 11). The early Carboniferous extension-related magmatism and the absence of coeval sedimentary successions may reflect the onset of asthenospheric upwelling and regional uplift, and therefore mark the initiation of the lithospheric extension. Nevertheless, the asthenospheric upwelling could be induced by either slab roll-back or slab break-off of the subducted PAO; more geological, geochemical, geophysical and palaeontological evidence is therefore needed to further constrain the specific tectonic setting of this extension, either back-arc or intra-continental.

7. Conclusions

The early Carboniferous (*c.* 332–326 Ma) granodiorite with high Sr/Y ratio, A-type monzogranite and A-type alkali-feldspar granite in the southwestern Alxa Block were most likely formed by partial melting of Neoarchean, Palaeoproterozoic and Mesoproterozoic crustal sources heated by upwelling asthenosphere in an lithospheric extensional setting. According to regional geological correlations, a uniform lithospheric extensional setting, either back-arc or intra-continental, but not a simple continental arc, is suggested for both the Alxa Block and the southeastern CAOB during early Carboniferous time, with the development of extension-related magmatism and the absence of coeval sedimentary rocks.

References

Andersen T (2002) Correction of common lead in U–Pb analyses that do not report [204]Pb. *Chemical Geology* **192**, 59–79.

Bao Q, Zhang C, Wu Z, Wang H, Li W, Sang J and Liu Y (2007) SHRIMP U-Pb zircon geochronology of a Carboniferous quartzdiorite in Baiyingaole area, Inner Mongolia and its implications. *Journal of Jilin University (Earth Science Edition)* **37**, 15–23 (in Chinese with English abstract).

Bickford ME, Schmus WR, Karlstrom KE, Mueller PA and Kamenov GD (2015) Mesoproterozoic-trans-Laurentian magmatism: a synthesis of continent-wide age distributions, new SIMS U–Pb ages, zircon saturation temperatures, and Hf and Nd isotopic compositions. *Precambrian Research* **265**, 286–312.

Blight JHS, Crowley QG, Petterson MG and Cunningham D (2010) Granites of the Southern Mongolia Carboniferous Arc: new geochronological and geochemical constraints. *Lithos* **116**, 35–52.

Bonin B (2007) A-type granites and related rocks: evolution of a concept, problems and prospects. *Lithos* **97**, 1–29.

Bu J, Niu Z, Wu J and Duan X (2012) Sedimentary characteristics and age of Amushan formation in Ejin Banner and its adjacent areas, western Inner Mongolia. *Geological Bulletin of China* **31**, 1669–83 (in Chinese with English abstract).

Chen W, Zhou W, Chen K, Liu M, Wang T, Fang M, He H and Zhang B (2013) Subduction-related Early Permian granodiorite in Jinchangshan of Alashan, Inner Mongolia: Evidences from zircon U-Pb geochronology and geochemistry. *Journal of Mineralogy and Petrology* **33**, 53–60 (in Chinese with English abstract).

Chen Y, Zhao R, Wang G, Rong X and Li T (2020) Geochronology, geochemical characteristics and significances of quartz monzonite in Niujiaogou, Longshoushan, Gansu. *Journal of East China University of Technology (Natural Science)* **43**, 21–29 (in Chinese with English abstract).

Coombs ML, Clague DA, Moore GF and Cousens BL (2004) Growth and collapse of Waianae Volcano, Hawaii, as revealed by exploration of its submarine flanks. *Geochemistry, Geophysics, Geosystems* **5**, Q05006, doi: 10.1029/2004GC000717.

Corfu F, Hanchar JM, Hoskin PWO and Kinny P (2003) Atlas of zircon textures. *Reviews in Mineralogy and Geochemistry* **53**, 469–500.

Cousens BL, Henry CD, Stevens C, Varve S, John DV and Wetmore S (2019) Igneous rocks in the Fish Creek Mountains and environs, Battle Mountain area, north-central Nevada: a microcosm of Cenozoic igneous activity in the northern Great Basin, Basin and Range Province, USA. *Earth-Science Reviews* **192**, 403–44.

Cui Y, Zhou H, Geng J, Li H and Li H (2012) In-site LA-MC-ICP-MS U–Pb isotopic dating of monazite. *Acta Geologica Sinica* **33**, 865–76 (in Chinese with English abstract).

Dan W, Li XH, Guo J, Liu Y and Wang XC (2012) Paleoproterozoic evolution of the eastern Alxa Block, westernmost North China: evidence from in situ zircon U–Pb dating and Hf–O isotopes. *Gondwana Research* **21**, 838–64.

Dan W, Li XH, Wang Q, Tang GJ and Liu Y (2014) An Early Permian (ca. 280 Ma) silicic igneous province in the Alxa Block, NW China: a magmatic flare-up triggered by a mantle-plume? *Lithos* **204**, 144–58.

Dan W, Li XH, Wang Q, Wang XC, Wyman DA and Liu Y (2016) Phanerozoic amalgamation of the Alxa Block and North China Craton: evidence from Paleozoic granitoids, U–Pb geochronology and Sr–Nd–Pb–Hf–O isotope geochemistry. *Gondwana Research* **32**, 105–21.

DeCelles PG, Ducea MN, Kapp P and Zandt G (2009) Cyclicity in Cordilleran Orogenic systems. *Nature Geoscience* **2**, 251–7.

DeCelles PG and Graham SA (2015) Cyclical processes in the North American Cordilleran Orogenic system. *Geology* **43**, 499–502.

Defant MJ and Drummond MS (1990) Derivation of some modern arc magmas by melting of young subducted lithosphere. *Nature* **347**, 662–5.

Depaolo DJ, Linn AM and Schubert G (1991) The continental crustal age distribution: methods of determining mantle separation ages from Sm-Nd isotopic data and application to the Southwestern United States. *Journal of Geophysical Research* **96**, 2071–88.

Duan J, Li C, Qian Z and Jiao J (2015) Geochronological and geochemical constraints on the petrogenesis and tectonic significance of Paleozoic dolerite dykes in the southern margin of Alxa Block, North China Craton. *Journal of Asian Earth Sciences* **111**, 244–53.

Ducea MN, Saleeby JB and Bergantz G (2015) The architecture, chemistry, and evolution of continental magmatic arcs. *Annual Review of Earth and Planetary Sciences* **43**, 10.1–10.33.

Eby GN (1990) The A-type granitoids: a review of their occurrence and chemical characteristics and speculations on their petrogenesis. *Lithos* **26**, 115–34.

Eby GN (1992) Chemical subdivision of A-type granitoids: petrogenesis and tectonic implications. *Geology* **20**, 641–4.

Eizenhöfer PR and Zhao G (2018) Solonker Suture in east Asia and its bearing on the final closure of the eastern segment of the Palaeo-Asian Ocean. *Earth-Science Reveiws* **186**, 153–72.

Geng Y, Wang X, Wu C and Zhou X (2010) Late-Paleoproterozoic tectono-thermal events of the metamorphic basement in Alxa area: evidence from geochronology. *Acta Petrologica Sinica* **26**, 1159–70 (in Chinese with English abstract).

Gong J, Zhang J, Wang Z, Yu S and Wang D (2018a) Late Ordovician–Carboniferous tectonic evolutionary history of the Alxa Block: constrained by the multistage magmatic-metamorphic-deformation events in Beidashan area. *Acta Petrologica et Mineralogica* 37, 771–98 (in Chinese with English abstract).

Gong J, Zhang J, Wang Z, Yu S, Wang D and Zhang H (2018b) Zircon U-Pb dating, Hf isotopic and geochemical characteristics of two suites of gabbros in the Beidashan region, western Alxa Block: its implications for evolution of the Central Asian Orogenic Belt. *Acta Geologica Sinica* 92, 1369–88 (in Chinese with English abstract).

Gong J, Zhang J and Yu S (2011) The origin of Longshoushan Group and associated rocks in the southern part of the Alxa Block: constraint from LA-ICP-MS U-Pb zircon dating. *Acta Petrologica et Mineralogica* 30, 795–818 (in Chinese with English abstract).

Gong J, Zhang J, Yu S, Li H and Hou K (2012) Ca. 2.5 Ga TTG rocks in the western Alxa Block and their implications. *Chinese Science Bulletin* 57, 4064–76 (in Chinese with English abstract).

Gu G (2012) The preliminary studies on the origin and tectonic setting of Early Mesozoic granites in the southwest margin of Alxa. M.Sc. thesis, Lanshou University, China. Published thesis (in Chinese with English abstract).

Han BF, He GQ, Wang XC and Guo ZJ (2011) Late Carboniferous collision between the Tarim and Kazakhstan–Yili terranes in the western segment of the South Tian Shan Orogen, Central Asia, and implications for the Northern Xinjiang, western China. *Earth-Science Reviews* 109, 74–93.

Han BF, Wang SG, Jahn BM, Hong DW, Kagami H and Sun YL (1997) Depleted-mantle source for the Ulungur River A-type granites from North Xinjiang, China: geochemistry and Nd–Sr isotopic evidence, and implications for Phanerozoic crustal growth. *Chemical Geology* 138, 135–59.

Han W, Liu X, Li J and Shi J (2012) Sedimentary environment of Carboniferous–Permian Amushan Formation in Wulanaobao area of Urad Rear Banner, Inner Mongolia. *Geological Bulletin of China* 31, 1684–91 (in Chinese with English abstract).

Huo Y (2019) Geochemical characteristics and geological significance of Late Paleozoic intrusive rocks in Ubud, Beidashan, Alxa. M.Sc. thesis, China University of Geosciences (Beijing), China (in Chinese with English abstract). Published thesis.

Jackson SE, Pearson NJ, Griffin WL and Belousova EA (2004) The application of laser ablation-inductively coupled plasma-mass spectrometry to in situ U–Pb zircon geochronology. *Chemical Geology* 211, 47–67.

Jahn BM, Bernard-Griffiths J, Charlot R, Cornichet J and Vidal F (1980) Nd and Sr isotopic compositions and REE abundances of Cretaceous MORB (Holes 417D and 418A, LEGS 51, 52 and 53). *Earth and Planetary Science Letters* 48, 171–184.

Jahn BM, Litvinovsky BA, Zanvilevich AN and Reichow M (2009) Peralkaline granitoid magmatism in the Mongolian–Transbaikalian Belt: evolution, petrogenesis and tectonic significance. *Lithos* 113, 521–39.

Jahn BM, Wu F and Hong D (2000) Important crustal growth in the Phanerozoic: isotopic evidence of granitoids from east-central Asia. *Journal of Earth System Science* 109, 5–20.

Ji Z, Ge WC, Yang H, Tian DX, Chen HJ and Zhang YL (2018) Late Carboniferous–Early Permian high- and low-Sr/Y granitoids of the Xing'an Block, northeastern China: implications for the late Paleozoic tectonic evolution of the eastern Central Asian Orogenic Belt. *Lithos* 322, 179–96.

Ji Z, Zhang Z, Yang J, Chen Y and Tang J (2020) Carboniferous–Early Permian sedimentary rocks from the north-eastern Erenhot, North China: implications on the tectono-sedimentary evolution of the south-eastern Central Asian Orogenic Belt. *Geological Journal* 55(3), 2383–401, doi: 10.1002/gj.3763.

Jian P, Kröner A, Windley BF, Shi Y, Zhang W, Zhang L and Yang W (2012) Carboniferous and Cretaceous mafic–ultramafic massifs in Inner Mongolia (China): A SHRIMP zircon and geochemical study of the previously presumed integral 'Hegenshan ophiolite'. *Lithos* 142–143, 48–66.

Jian P, Liu D, Kröner A, Windley BF, Shi Y, Zhang W, Zhang F, Miao L, Zhang L and Tomurhuu D (2010) Evolution of a Permian intraoceanic arc–trench system in the Solonker suture zone, Central Asian Orogenic Belt, China and Mongolia. *Lithos* 118, 169–90.

Jiao J, Jin S, Rui H, Zhang G, Ning Q and Shao L (2017) Petrology, geochemistry and chronology study of the Xiaokouzi mafic-ultramafic intrusion in the eastern section of Longshou Mountains, Gansu. *Acta Geologica Sinica* 91, 736–47 (in Chinese with English abstract).

Karsli O, Caran Ş, Dokuz A, Çoban H, Chen B and Kandemir R (2012) A-type granitoids from the Eastern Pontides, NE Turkey: records for generation of hybrid A-type rocks in a subduction-related environment. *Tectonophysics* 530–531, 208–24.

King PL, White AJR, Chappell BW and Allen CM (1997) Characterization and origin of aluminous A-type granites from the Lachlan Fold Belt, southeastern Australia. *Journal of Petrology* 38, 371–91.

Kozlovsky AM, Yarmolyuk VV, Salnikova EB, Travin AV, Kotov AB, Plotkina JV, Kudryashova EA and Savatenkov VM (2015) Late Paleozoic anorogenic magmatism of the Gobi Altai (SW Mongolia): tectonic position, geochronology and correlation with igneous activity of the Central Asian Orogenic Belt. *Journal of Asian Earth Sciences* 113, 524–41.

Li J, Zhang J and Qu J (2012a) Amalgamation of the North China Craton with Alxa Block in the late of Early Paleozoic: evidence from sedimentary sequences in the Niushou Mountain, Ningxia Hui Autonomous Region, NW China. *Geological Review* 58, 208–14 (in Chinese with English abstract).

Li P, Zhang S, Gao R, Li H, Zhao Q, Li Q and Guan Y (2012b) New Upper Carboniferous–Lower Permian paleomagnetic results from the central Inner Mongolia and their geological implications. *Journal of Jilin University (Earth Science Edition)* 42, 423–40 (in Chinese with English abstract).

Li Y, Wang G, Santosh M, Wang J, Dong P and Li H (2018) Supra-subduction zone ophiolites from Inner Mongolia, North China: Implications for the tectonic history of the southeastern Central Asian Orogenic Belt. *Gondwana Research* 59, 126–43.

Lin L, Xiao WJ, Wan B, Windley BF, Ao S, Han C, Feng J, Zhang J and Zhang Z (2014) Geochronologic and geochemical evidences for persistence of south-dipping subduction to Late Permian time, Langshan area, Inner Mongolia (China): significance for termination of accretionary orogenesis in the southern Altaids. *American Journal of Science* 314, 679–703.

Liu J, Chi X, Zhang X, Ma Z, Zhao Z, Wang T, Hu Z and Zhao X (2009) Geochemical characteristic of Carboniferous quartz-diorite in the southern Xiwuqi area, Inner Mongolia and its tectonic significance. *Acta Geologica Sinica* 83, 365–76 (in Chinese with English abstract).

Liu M, Zhang D, Xiong G, Zhao H, Di Y, Wang Z and Zhou Z (2016a) Zircon U–Pb age, Hf isotope and geochemistry of Carboniferous intrusions from the Langshan area, Inner Mongolia: petrogenesis and tectonic implications. *Journal of Asian Earth Sciences* 120, 139–58.

Liu Q, Zhao G, Han Y, Eizenhöfer PR, Zhu Y, Hou W, Zhang X and Wang B (2017) Geochronology and geochemistry of Permian to Early Triassic granitoids in the Alxa Terrane: constraints on the final closure of the Paleo-Asian Ocean. *Lithosphere* 9, L646.641.

Liu Q, Zhao G, Sun M, Han Y, Eizenhöfer PR, Hou W, Zhang X, Zhu Y, Wang B, Liu D and Xu B (2016b) Early Paleozoic subduction processes of the Paleo-Asian Ocean: insights from geochronology and geochemistry of Paleozoic plutons in the Alxa Terrane. *Lithos* 262, 546–60.

Liu W, Pan J, Liu X, Wang K, Wang G and Xue P (2019) Petrogenesis and tectonic implication of Qingshanbao pluton in Longshou Moutains, Gansu: constraints from elemental geochemistry, zircon U–Pb age and Sr-Nd isotopes. *Journal of Mineralogy and Petrology* 39, 26–40 (in Chinese with English abstract).

Ludwig KR (2012) *User's Manual for Isoplot 3.75: A Geochronological Toolkit for Microsoft Excel.* Berkeley: Berkeley Geochronology Center, Special Publication no. 5, 75 pp.

Luo ZW, Xu B, Shi GZ, Zhao P, Faure M and Chen Y (2016) Solonker ophiolite in Inner Mongolia, China: a late Permian continental margin-type ophiolite. *Lithos* 261, 72–91.

Maniar PD and Piccoli PM (1989) Tectonic discrimination of granitoids. *Geological Society of America Bulletin* 101, 635–43.

Martin H, Smithies RH, Rapp R, Moyen JF and Champion D (2005) An overview of adakite, tonalite–trondhjemite–granodiorite (TTG), and sanukitoid: relationships and some implications for crustal evolution. *Lithos* 79, 1–24.

Moyen JF (2009) High Sr/Y and La/Yb ratios: the meaning of the 'adakitic signature'. *Lithos* 112, 556–74.

Murphy JB (2013) Appinite suites: a record of the role of water in the genesis, transport, emplacement and crystallization of magma. *Earth-Science Reviews* **119**, 35–59.

Pan X (2019) Petrogenesis of Tebai basic-ultrabasic pluton in the Beidashan area in the southern margin of the Alxa block and its tectonic significance. M.Sc. thesis, Chang'an University, China. Published thesis (in Chinese with English abstract).

Pang CJ, Wang XC, Xu B, Luo ZW and Liu YZ (2017) Hydrous parental magmas of Early to Middle Permian gabbroic intrusions in western Inner Mongolia, North China: new constraints on deep-Earth fluid cycling in the Central Asian Orogenic Belt. *Journal of Asian Earth Sciences* **144**, 184–204.

Pang CJ, Wang XC, Xu B, Zhao JX, Feng YX, Wang YY, Luo ZW and Liao W (2016) Late Carboniferous N-MORB-type basalts in central Inner Mongolia, China: products of hydrous melting in an intraplate setting? *Lithos* **261**, 55–71.

Pearce JA (1996) Source and settings of granitic rocks. *Episodes* **19**, 120–5.

Pearce JA and Norry MJ (1979) Petrogenetic implications of Ti, Zr, Y, and Nb variations in volcanic rocks. *Contributions to Mineralogy and Petrology* **69**, 33–47.

Pruner P (1992) Palaeomagnetism and palaeogeography of Mongolia from the Carboniferous to the Cretaceous—final report. *Physics of the Earth and Planetary Interiors* **70**, 169–77.

Qin H (2012) Petrology of Early Paleozoic granites and their relation to tectonic evolution of orogen in the North Qilian Orogenic Belt. Ph.D. thesis, Chinese Academy of Geological Sciences, China. Published thesis (in Chinese with English abstract).

Rudnick RL and Gao S (2003) Composition of the continental crust. In *Treatise on Geochemistry*, volume 3 (eds HD Holland and KK Turekian), pp. 1–64. Amsterdam: Elsevier Science Ltd.

Sain A, Saha D, Joy S, Jelsma H and Armstrong R (2017) New SHRIMP age and microstructures from a deformed A-type granite, Kanigiri, Southern India: constraining the Hiatus between orogenic closure and postorogenic rifting. *The Journal of Geology* **125**, 241–59.

Saunders AD, Storey M, Kent RW and Norry MJ (1992) Consequences of plume-lithosphere interactions. In *Magmatism and the Causes of Continental Break-up* (eds BC Storey, T Alabaster and RJ Pankhurst), pp. 41–60. Geological Society of London, Special Publication no. **68**.

Shervais JW (1982) Ti-V plots and the petrogenesis of modern and ophiolitic lavas. *Earth and Planetary Science Letters* **59**, 101–18.

Shi G, Song G, Wang H, Huang C, Zhang L and Tang J (2016) Late Paleozoic tectonics of the Solonker Zone in the Wuliji area, Inner Mongolia, China: insights from stratigraphic sequence, chronology, and sandstone geochemistry. *Journal of Asian Earth Sciences* **127**, 100–18.

Sláma J, Košler J, Condon DJ, Crowley JL, Gerdes A, Hanchar JM, Horstwood MSA, Morris GA, Nasdala L, Tubrett MN and Whitehouse MJ (2008) Plešovice zircon–A new natural reference material for U–Pb and Hf isotopic microanalysis. *Chemical Geology* **249**, 1–35.

Song D, Xiao W, Collins A, Glorie S and Han C (2019) Late Carboniferous–Early Permian arc magmatism in the southwestern Alxa Tectonic Belt (NW China): constraints on the Late Palaeozoic subduction history of the Paleo-Asian Ocean. *Geological Journal* **54**, 1046–63.

Song D, Xiao W, Collins AS, Glorie S, Han C and Li Y (2017) New chronological constrains on the tectonic affinity of the Alxa Block, NW China. *Precambrian Research* **299**, 230–43.

Song D, Xiao W, Collins AS, Glorie S, Han C and Li Y (2018) Final subduction processes of the Paleo-Asian Ocean in the Alxa Tectonic Belt (NW China): constraints from field and chronological data of Permian arc-related volcano-sedimentary rocks. *Tectonics* **37**, 1658–87.

Song S, Niu Y, Su L and Xia X (2013) Tectonics of the North Qilian orogen, NW China. *Gondwana Research* **23**, 1378–401.

Sun SS and McDonough W (1989) Chemical and isotopic systematics of oceanic basalts: implications for mantle composition and processes. In *Magmatism in the Ocean Basins* (eds AD Saunders and MJ Norry), pp. 313–45. Geological Society of London, Special Publication no. **42**.

Tang L (2015) Granites' characteristics and zircon LA-ICP-MS U-Pb dating of Jiling area in Longshoushan, Gansu province. M.Sc. thesis, East China Institute of Technology, China. Published thesis (in Chinese with English abstract).

Tang S, Li J, Liang X, Zhang L, Li G, Pu W, Li C, Yang Y, Chu Z, Zhang J, Hou K and Wang X (2017) Reference material preparation of $^{143}Nd/^{144}Nd$ isotope ratio. *Rock and Mineral Analysis* **36**, 163–70 (in Chinese with English abstract)

Tang S, Li J, Pan CX, Liu H and Yan B (2021) Production and certification of the reference material GBW04139, GBW04140 and GBW04141 as Rb-Sr and Sm-Nd isotope analysis references. *Rock and Mineral Analysis* **40**, 284–94 (in Chinese with English abstract).

Tong Y, Jahn BM, Wang T, Hong DW, Smith EI, Sun M, Gao JF, Yang QD and Huang W (2015) Permian alkaline granites in the Erenhot–Hegenshan belt, northern Inner Mongolia, China: model of generation, time of emplacement and regional tectonic significance. *Journal of Asian Earth Sciences* **97**, Part B, 320–36.

Tung K, Yang H, Liu D, Zhang J, Tseng C and Wan Y (2007) SHRIMP U-Pb geochronology of the detrital zircons from the Longshoushan Group and its tectonic significance. *Chinese Science Bulletin* **52**, 1414–25.

Wan Y, Song B, Liu D, Wilde SA, Wu J, Shi Y, Yin X and Zhou H (2006) SHRIMP U–Pb zircon geochronology of Palaeoproterozoic metasedimentary rocks in the North China Craton: evidence for a major Late Palaeoproterozoic tectonothermal event. *Precambrian Research* **149**, 249–71.

Wang J, Li X, Ning W, Kusky T and Deng H (2019a) Geology of a Neoarchean suture: evidence from the Zunhua ophiolitic mélange of the Eastern Hebei Province, North China Craton. *Geological Society of America Bulletin* **131**, 11–2.

Wang XC, Wilde SA, Li QL and Yang YN (2015a) Continental flood basalts derived from the hydrous mantle transition zone. *Nature Communications* **6**, 7700, doi: 10.1038/ncomms8700.

Wang XC, Wilde SA, Xu B and Pang CJ (2016a) Origin of arc-like continental basalts: implications for deep-Earth fluid cycling and tectonic discrimination. *Lithos* **261**, 5–45.

Wang Y, Xu B, Song S, Zhao P, Zhang J and Yan L (2021a) A late Paleozoic extension basin constrained by sedimentology and geochronology in eastern Central Asia Orogenic Belt. *Gondwana Research* **89**, 265–86.

Wang ZZ, Chen X, Li B, Zhang Y and Xu S (2019b) The discovery of the Paleoproterozoic syenite in Helishan, Gansu Province, and its implications for the tectonic attribution of the Alxa Block. *Geology in China* **46**, 1094–104 (in Chinese with English abstract).

Wang ZZ, Chen X, Shao Z, Li B, Ding W, Zhang Y, Wang Y, Zhang Y, Xu S and Qin X (2020) Petrogenesis of the Late Silurian–Early Devonian granites in the Longshoushan–Helishan area, Gansu Province, and its tectonic implications for the Early Paleozoic evolution of the southwestern Alxa Block. *Acta Geologica Sinica* **94**, 2243–61 (in Chinese with English abstract).

Wang ZZ, Han BF, Feng LX and Liu B (2015b) Geochronology, geochemistry and origins of the Paleozoic–Triassic plutons in the Langshan area, western Inner Mongolia, China. *Journal of Asian Earth Sciences* **97**, Part B, 337–51.

Wang ZZ, Han BF, Feng LX, Liu B, Zheng B and Kong LJ (2016b) Tectonic attribution of the Langshan area in western Inner Mongolia and implications for the Neoarchean–Paleoproterozoic evolution of the western North China Craton: evidence from LA-ICP-MS zircon U–Pb dating of the Langshan basement. *Lithos* **261**, 278–95.

Wang ZZ, Han BF, Feng LX, Liu B, Zheng B, Kong LJ and Qi CY (2021b) Early–Middle Permian plutons in the Langshan area, western Inner Mongolia, China, and their tectonic implications. *Lithos* **382–383**, 105934.

Wei Q, Hao L, Lu J, Zhao Y, Zhao X and Shi H (2013) LA-MC-ICP-MS zircon U-Pb dating of Hexipu granite and its geological implications. *Bulletin of Mineralogy, Petrology and Geochemistry* **32**, 729–35 (in Chinese with English abstract).

Whalen J, Currie K and Chappell B (1987) A-type granites: geochemical characteristics, discrimination and petrogenesis. *Contributions to Mineralogy and Petrology* **95**, 407–19.

Whitaker ML, Nekvasil H, Lindsley DH and McCurry M (2008) Can crystallization of olivine tholeiite give rise to potassic rhyolites?—an experimental investigation. *Bulletin of Volcanology* **70**, 417–34.

Wilde SA & Zhou JB (2015) The late Paleozoic to Mesozoic evolution of the eastern margin of the Central Asian Orogenic Belt in China. *Journal of Asian Earth Sciences* **113**, 909–21.

Windley BF, Alexeiev D, Xiao W, Kröner A and Badarch G (2007) Tectonic models for accretion of the Central Asian Orogenic Belt. *Journal of the Geological Society* **164**, 31–47.

Wu FY, Jahn BM, Wilde SA, Lo CH, Yui TF, Lin Q, Ge WC and Sun DY (2003) Highly fractionated I-type granites in NE China (II): isotopic geochemistry and implications for crustal growth in the Phanerozoic. *Lithos* **67**, 191–204.

Wu FY, Sun DY, Li H, Jahn BM and Wilde S (2002) A-type granites in northeastern China: age and geochemical constraints on their petrogenesis. *Chemical Geology* **187**, 143–73.

Xia LQ (2014) The geochemical criteria to distinguish continental basalts from arc related ones. *Earth-Science Reviews* **139**, 195–212.

Xiao W, Windley BF, Han C, Liu W, Wan B, Zhang Je, Ao S, Zhang Z and Song D (2018) Late Paleozoic to early Triassic multiple roll-back and oroclinal bending of the Mongolia collage in Central Asia. *Earth-Science Reviews* **186**, 94–128.

Xiao W, Windley BF, Jie H and Zhai M (2003) Accretion leading to collision and the Permian Solonker suture, Inner Mongolia, China: termination of the central Asian orogenic belt. *Tectonics* **22**, 1–20.

Xiao W, Windley BF, Yong Y, Yan Z, Yuan C, Liu C and Li J (2009a) Early Paleozoic to Devonian multiple-accretionary model for the Qilian Shan, NW China. *Journal of Asian Earth Sciences* **35**, 323–33.

Xiao WJ, Windley BF, Huang BC, Han CM, Yuan C, Chen HL, Sun M, Sun S and Li JL (2009b) End-Permian to mid-Triassic termination of the accretionary processes of the southern Altaids: implications for the geodynamic evolution, Phanerozoic continental growth, and metallogeny of Central Asia. *International Journal of Earth Sciences* **98**, 1189–217.

Xu B, Charvet J, Chen Y, Zhao P and Shi G (2013) Middle Paleozoic convergent orogenic belts in western Inner Mongolia (China): framework, kinematics, geochronology and implications for tectonic evolution of the Central Asian Orogenic Belt. *Gondwana Research* **23**, 1342–64.

Xu B, Wang Z, Zhang L, Wang Z, Yang Z and He Y (2018) The Xing-Meng intracontinent orogenic belt. *Acta Petrologica Sinica* **34**, 2819–44 (in Chinese with English abstract).

Xu B, Zhao P, Bao Q, Zhou Y, Wang Y and Luo Z (2014) Preliminary study on the pre-Mesozoic tectonic unit division of the Xing-Meng Orogenic Belt (XMOB). *Acta Petrologica Sinica* **30**, 1841–57 (in Chinese with English abstract).

Xue S, Ling MX, Liu YL, Zhang H and Sun W (2017) The genesis of early Carboniferous adakitic rocks at the southern margin of the Alxa Block, North China. *Lithos* **278–281**, 181–94.

Yang JH, Wu FY, Chung SL, Wilde SA and Chu MF (2006) A hybrid origin for the Qianshan A-type granite, northeast China: geochemical and Sr–Nd–Hf isotopic evidence. *Lithos* **89**, 89–106.

Yang JH, Wu FY, Wilde SA, Xie LW, Yang YH and Liu XM (2007) Tracing magma mixing in granite genesis: in situ U–Pb dating and Hf-isotope analysis of zircons. *Contributions to Mineralogy & Petrology* **153**, 177–90.

Yin H, Zhou H, Zhang W, Zheng X and Wang S (2016) Late Carboniferous to early Permian sedimentary–tectonic evolution of the north of Alxa, Inner Mongolia, China: evidence from the Amushan Formation. *Geoscience Frontiers* **7**, 733–41.

Yuan W and Yang Z (2015) The Alashan Terrane was not part of North China by the Late Devonian: evidence from detrital zircon U–Pb geochronology and Hf isotopes. *Gondwana Research* **27**, 1270–82.

Zhang B, Zhang J, Zhang Y, Zhao H, Wang Y and Nie F (2016a) Tectonic affinity of the Alxa Block, Northwest China: constrained by detrital zircon U–Pb ages from the early Paleozoic strata on its southern and eastern margins. *Sedimentary Geology* **339**, 289–303.

Zhang D, Huang B, Zhao Q and Zhang Y (2018a) Paleomagnetic results from Lower Devonian sandstones of the Niqiuhe Formation in the Duobaoshan area and its constraints on paleoposition of the Xing'an block. *Chinese Science Bulletin* **63**, 1502–14 (in Chinese with English abstract).

Zhang J and Gong J (2018) Revisiting the nature and affinity of the Alxa Block. *Acta Petrologica Sinica* **34**, 940–62 (in Chinese with English abstract).

Zhang J, Gong J, Yu S, Li H and Hou K (2013a) Neoarchean–Paleoproterozoic multiple tectonothermal events in the western Alxa block, North China Craton and their geological implication: evidence from zircon U–Pb ages and Hf isotopic composition. *Precambrian Research* **235**, 36–57.

Zhang J, Li J, Xiao W, Wang Y and Qi W (2013b) Kinematics and geochronology of multistage ductile deformation along the eastern Alxa block, NW China: new constraints on the relationship between the North China Plate and the Alxa block. *Journal of Structural Geology* **57**, 38–57.

Zhang J, Wang T, Castro A, Zhang L, Shi X, Tong Y, Zhang Z, Guo L, Yang Q and Iaccheri LM (2016b) Multiple mixing and hybridization from magma source to final emplacement in the Permian Yamatu Pluton, the northern Alxa Block, China. *Journal of Petrology* **57**, 933–80.

Zhang J, Wei C and Chu H (2015a) Blueschist metamorphism and its tectonic implication of Late Paleozoic–Early Mesozoic metabasites in the mélange zones, central Inner Mongolia, China. *Journal of Asian Earth Sciences* **97**, Part B, 352–64.

Zhang J, Wei C and Chu H (2018b) New model for the tectonic evolution of Xing'an-Inner Mongolia Orogenic Belt: evidence from four different phases of metamorphism in Central Inner Mongolia. *Acta Petrologica Sinica* **34**, 2857–572 (in Chinese with English abstract).

Zhang J, Zhang B and Zhao H (2016c) Timing of amalgamation of the Alxa Block and the North China Block: constraints based on detrital zircon U–Pb ages and sedimentologic and structural evidence. *Tectonophysics* **668–669**, 65–81.

Zhang L, Zhang H, Zhang S, Xiong Z, Luo B, Yang H, Pan F, Zhou X, Xu W and Guo L (2017a) Lithospheric delamination in post-collisional setting: evidence from intrusive magmatism from the North Qilian orogen to southern margin of the Alxa block, NW China. *Lithos* **288–289**, 20–34.

Zhang Q, Liu Z, Chai S, Xu Z, Zhao Q and Xu X (2011) Geochronology and geochemistry of granodiorites from Wulan area of Urad Zhongqi, Inner Mongolia. *Journal of Mineralogy and Petrology* **31**, 7–14 (in Chinese with English abstract).

Zhang S and Zhao Y (2017) Cogenetic origin of mafic microgranular enclaves in calc-alkaline granitoids: the Permian plutons in the northern North China Block. *Geosphere* **13**, 482–517.

Zhang SH, Zhao Y, Liu JM and Hu ZC (2016d) Different sources involved in generation of continental arc volcanism: the Carboniferous–Permian volcanic rocks in the northern margin of the North China block. *Lithos* **240–243**, 382–401.

Zhang SH, Zhao Y, Song B, Yang ZY, Hu JM and Wu H (2007) Carboniferous granitic plutons from the northern margin of the North China block: implications for a late Palaeozoic active continental margin. *Journal of the Geological Society* **164**, 451–63.

Zhang SH, Zhao Y, Ye H, Liu JM and Hu ZC (2014) Origin and evolution of the Bainaimiao arc belt: implications for crustal growth in the southern Central Asian orogenic belt. *GSA Bulletin* **126**, 1275–300.

Zhang X, Gao Y, Wang Z, Liu H and Ma Y (2012a) Carboniferous appinitic intrusions from the northern North China Craton: geochemistry, petrogenesis and tectonic implications. *Journal of the Geological Society* **169**, 337–51.

Zhang X, Xue F, Yuan L, Ma Y and Wilde SA (2012b) Late Permian appinite–granite complex from northwestern Liaoning, North China Craton: petrogenesis and tectonic implications. *Lithos* **155**, 201–17.

Zhang X, Yuan L, Xue F, Yan X and Mao Q (2015b) Early Permian A-type granites from central Inner Mongolia, North China: magmatic tracer of post-collisional tectonics and oceanic crustal recycling. *Gondwana Research* **28**, 311–27.

Zhang Y, Niu Y, Wei J, Shi J and Song B (2018c) Chronology of the Haobiru Formation in the Haobiru area of northern Alxa, Inner Mongolia and its geological implications. *Geological Bulletin of China* **37**, 51–62 (in Chinese with English abstract).

Zhang Z, Chen Y, Li K, Li J, Yang J and Qian X (2017b) Geochronology and geochemistry of Permian bimodal volcanic rocks from central Inner Mongolia, China: implications for the late Palaeozoic tectonic evolution of the south-eastern Central Asian Orogenic Belt. *Journal of Asian Earth Sciences* **135**, 370–89.

Zhang Z, Li K, Li J, Tang W, Chen Y and Luo Z (2015c) Geochronology and geochemistry of the Eastern Erenhot ophiolitic complex: implications for the tectonic evolution of the Inner Mongolia–Daxinganling Orogenic Belt. *Journal of Asian Earth Sciences* **97**, 279–93.

Zhang Z, Wang K, Wang G, Liu X, Liu W and Wu B (2018d) Petrogenesis and tectonic significances of the Paleozoic Jiling syenite in the mountain

Longshou area, Gansu province. *Geological Review* **64**, 1017–29 (in Chinese with English abstract).

Zhao G, Cawood PA, Li S, Wilde SA, Sun M, Zhang J, He Y and Yin C (2012) Amalgamation of the North China Craton: key issues and discussion. *Precambrian Research* **222–223**, 55–76.

Zhao G, Sun M, Wilde SA and Li SZ (2005) Late Archean to Paleoproterozoic evolution of the North China Craton: key issues revisited. *Precambrian Research* **136**, 177–202.

Zhao G, Wang Y, Huang B, Dong Y, Li S, Zhang G and Yu S (2018) Geological reconstructions of the East Asian blocks: from the breakup of Rodinia to the assembly of Pangea. *Earth-Science Reviews* **186**, 262–86.

Zhao P, Chen Y, Xu B, Faure M, Shi G and Choulet F (2013) Did the Paleo-Asian Ocean between North China Block and Mongolia Block exist during the late Paleozoic? First paleomagnetic evidence from central-eastern Inner Mongolia, China. *Journal of Geophysical Research: Solid Earth* **118**, 1873–94.

Zhao P, Jahn BM, Xu B, Liao W and Wang Y (2016a) Geochemistry, geochronology and zircon Hf isotopic study of peralkaline-alkaline intrusions along the northern margin of the North China Craton and its tectonic implication for the southeastern Central Asian Orogenic Belt. *Lithos* **261**, 92–108.

Zhao P, Xu B, Tong Q, Chen Y and Faure M (2016b) Sedimentological and geochronological constraints on the Carboniferous evolution of central Inner Mongolia, southeastern Central Asian Orogenic Belt: Inland sea deposition in a post-orogenic setting. *Gondwana Research* **31**, 253–70.

Zhao P, Xu B and Zhang C (2017) A rift system in southeastern Central Asian Orogenic Belt: constraint from sedimentological, geochronological and geochemical investigations of the Late Carboniferous-Early Permian strata in northern Inner Mongolia (China). *Gondwana Research* **47**, 342–57.

Zhao X, Liu C, Wang J, Zhang S and Guan Y (2020) Geochemistry, geochronology and Hf isotope of granitoids in the northern Alxa region: implications for the Late Paleozoic tectonic evolution of the Central Asian Orogenic Belt. *Geoscience Frontiers* **11**, 1711–25.

Zheng R, Li J, Xiao W and Wang L (2018) A new ophiolitic mélange containing boninitic blocks in Alxa region: implications for Permian subduction events in southern CAOB. *Geoscience Frontiers* **9**, 1355–67.

Zheng R, Li J, Zhang J, Xiao W and Li Y (2019) Early Carboniferous high Ba-Sr granitoid in southern Langshan of northeastern Alxa: implications for accretionary tectonics along the southern Central Asian Orogenic Belt. *Acta Geologica Sinica (English Edition)* **93**, 820–44.

Zheng R, Wu T, Zhang W, Xu C, Meng Q and Zhang Z (2014) Late Paleozoic subduction system in the northern margin of the Alxa block, Altaids: geochronological and geochemical evidences from ophiolites. *Gondwana Research* **25**, 842–58.

Zhou JB, Wilde SA, Zhao GC and Han J (2018) Nature and assembly of microcontinental blocks within the Paleo-Asian Ocean. *Earth-Science Reviews* **186**, 76–93.

Zhou XC, Zhang HF, Luo BJ, Pan FB, Zhang SS and Guo L (2016) Origin of high Sr/Y-type granitic magmatism in the southwestern of the Alxa Block, Northwest China. *Lithos* **256–257**, 211–27.

Zhou Z, Zhang H, Liu H, Liu C and Liu W (2009) Zircon U-Pb dating of basic intrusions in Siziwangqi area of middle Inner Mongolia, China. *Acta Petrologica Sinica* **25**, 1519–28 (in Chinese with English abstract).